

1

Title page

2 **Title:**

3 A 12 kb multi-allelic copy number variation encompassing a GC gene enhancer is associated with mastitis resistance in dairy
4 cattle

5 **Authors:**

6 Young-Lim Lee^{1*}, Haruko Takeda², Gabriel Costa Monteiro Moreira², Latifa Karim³, Erik Mullaart⁴, Wouter Coppieters^{2,3}, The
7 GplusE consortium⁵, Ruth Appeltant², Roel F. Veerkamp¹, Martien A. M. Groenen¹, Michel Georges², Mirte Bosse¹, Tom
8 Druet², Aniek C. Bouwman¹, Carole Charlier²

9 **Affiliations:**

10 ¹Wageningen University & Research, Animal Breeding and Genomics, Wageningen, the Netherlands

11 ²Unit of Animal Genomics, GIGA-R & Faculty of Veterinary Medicine, University of Liège, Liège, Belgium

12 ³GIGA Genomics Platform, GIGA Institute, University of Liège, Liège, Belgium

13 ⁴CRV B.V., Arnhem, the Netherlands

14 ⁵<http://www.gpluse.eu/>

15

16 * younglim.lee@wur.nl

17

18 **Abstract**

19 Clinical mastitis (CM) is an inflammatory disease occurring in the mammary glands of lactating cows. CM is under genetic control,
20 and a prominent CM resistance QTL located on chromosome 6 was reported in various dairy cattle breeds. Nevertheless, the
21 biological mechanism underpinning this QTL has been lacking. Herein, we mapped, fine-mapped, and discovered the putative causal
22 variant underlying this CM resistance QTL in the Dutch dairy cattle population. We identified a ~12 kb multi-allelic copy number
23 variant (CNV), that is in perfect linkage disequilibrium with a GWAS lead SNP, as a promising candidate variant. By implementing a
24 genome-wide association study (GWAS) and through expression QTL mapping, we showed that the group-specific component gene
25 (*GC*), a gene encoding a vitamin D binding protein, is an excellent candidate causal gene for the QTL. The multiplied alleles are
26 associated with increased *GC* expression and low CM resistance. Ample evidence from functional genomics data supports the
27 presence of an enhancer within this CNV, which would exert *cis*-regulatory effect on *GC*. We observed that strong positive selection
28 swept the region near the CNV, and haplotypes associated with the multiplied allele were strongly selected for. Moreover, the
29 multiplied allele showed pleiotropic effects for increased milk yield and reduced fertility, hinting that a shared underlying biology
30 for these effects may revolve around the vitamin D pathway. These findings together suggest a putative causal variant of a CM
31 resistance QTL, where a *cis*-regulatory element located within a CNV can alter gene expression and affect multiple economically
32 important traits.

33

34

35 Author summary

36 Clinical mastitis (CM) is an inflammatory disease that negatively influences dairy production and compromises animal welfare.
37 Although one major genetic locus for CM resistance was mapped on bovine chromosome 6, a mechanistic description of this
38 association has been lacking. Herein, we report a 12-kb multiallelic copy number variant (CNV), encompassing a strong
39 enhancer for group-specific component gene (*GC*), as a likely causal variant for this locus. This CNV is associated with high *GC*
40 expression and low CM resistance. We speculate that upregulation of *GC* leads to a large amount of vitamin D binding protein,
41 which in turn, reduces biologically available vitamin D, resulting in vitamin D deficiency and low CM resistance. Despite the
42 negative effect on CM resistance, the CNV contributes to increased milk production, hinting at balancing selection. Our results
43 highlight how multiplication of a regulatory element can shape economically important traits in dairy cattle, both in
44 favourable and unfavourable directions.

45

46 Introduction

47 Clinical mastitis (CM) is an inflammation in the mammary glands. This condition is often seen in dairy cattle and the
48 repercussions of CM include production loss, use of antibiotics, and compromised animal welfare [1]. CM resistance has a
49 genetic component, with estimated heritabilities ranging between 0.01 and 0.10 [2–6]. Genome-wide associations studies
50 (GWASs) identified several quantitative trait loci (QTL) associated with CM resistance or somatic cell score (SCS), an indicator
51 trait of CM. For instance, the six most significant CM resistance QTLs together capture 8.9% of the genetic variance in Danish
52 Holstein Friesian (HF) cattle, underlining the polygenic nature of CM resistance [7]. Of these six QTLs, the most significant QTL
53 mapped near 88 Mb on the Bos taurus autosome (BTA) 6 was repeatedly reported in various dairy cattle populations [8–12].
54 Several fine-mapping studies, using imputed whole genome sequence (WGS) variants, reported non-coding candidate causal
55 SNPs at the group-specific component (*GC*) gene [7,12–15]. One of these studies investigated, albeit unsuccessfully, whether
56 one of the non-coding candidate SNP obtained from the GWAS was associated with *GC* expression, leaving the functional
57 mechanisms underlying this association elusive [13]. Interestingly, the proposed candidate SNPs showed antagonistic allele
58 effects for milk yield (MY) (the high CM resistance allele was linked to low MY, and vice versa [7,13,16]), and one study
59 concluded that a single pleiotropic variant regulates both of the traits [17]. Furthermore, this locus harbours QTL for many
60 traits including body conformation, fertility, and longevity [12,15,18–22], implying pleiotropy, which remains to be
61 investigated. Until now, *GC*, a gene that encodes the vitamin D binding protein (DBP), has been considered the most promising
62 candidate gene for the CM resistance QTL on BTA 6 [13,14]. A growing body of literature underpins the importance of DBP,
63 which acts as a macrophage activating factor, modulates immune responses [23], and is central to the vitamin D pathway
64 [24]. For instance, polymorphisms in *GC* have been shown to cause vitamin D deficiency and inflammatory diseases in humans
65 [25]. Moreover, a therapeutic use of vitamin D in lactating, CM-infected cows reduced inflammation, implying a link between
66 vitamin D and inflammation [26,27]. Yet, the GWAS lead SNP was not associated with *GC* expression or alternative
67 transcription, leaving the functional mechanism elusive [13]. Some researchers hypothesized that a copy number variant
68 (CNV) might be the causal variant underlying this QTL [7]. Indeed, a CNV in high linkage disequilibrium (LD) with the GWAS
69 lead SNP was found in the 3' alternative exon of *GC*, however, the functional role of this CNV was not well characterized [13].
70 In this study, we aimed at confirming the presence of the prominent CM resistance QTL in the Dutch HF population, and
71 identifying a candidate causal gene and a variant that may explain the functional mechanism(s) of the QTL. Our findings
72 strongly suggest that (1) the CM resistance QTL on BTA 6 is present in the Dutch HF population; (2) a 12-kb multi-allelic CNV,
73 encompassing the 3' alternative exon of *GC*, harbours a putative enhancer, which exerts *cis*-regulation on the candidate
74 causal gene, *GC*; (3) a haplotype associated with the CNV allele is strongly selected for, and the CNV has pleiotropic effects
75 on MY, body conformation and fertility traits. These findings together highlight a functional CNV that contains a *cis*-regulatory
76 element, affecting gene expression and subsequently altering the economically important traits.

77 Results

78 A major CM resistance QTL on BTA 6 segregates in the Dutch HF cattle population

79 A CM resistance QTL has been identified on BTA6 in several cattle populations [7–10,12–14]. We first aimed at confirming
80 presence of this QTL in the Dutch HF population. All analyses were performed according to the Bovine genome assembly
81 UMD3.1 [28], unless noted otherwise. To map the QTL, we performed a GWAS using 4,142 progeny tested bulls. These
82 animals were genotyped using a custom 16K array, and imputed sequentially, firstly to the Illumina Bovine 50K array, and
83 then to higher density (770K). CM resistance was recorded as a binary trait, depending on the disease status registration
84 done by farmers [29]. The estimated breeding values of CM resistance were de-regressed and used as phenotypes in a single
85 SNP GWAS performed using an additive model, and accounting for genetic relationships. The strong association signal near
86 BTA 6:88.6 Mb found in Danish HF and Norwegian Red populations was replicated in the Dutch HF population ($-\log_{10}P=7.35$;
87 Fig 1A, S1 Fig). This association signal was found downstream of *GC*, a reverse-oriented gene located at BTA 6:88.68–88.74
88 Mb. We fine-mapped this QTL, using 45,782 imputed WGS level variants present in a 10-Mb window encompassing the QTL
89 (BTA 6:84–93 Mb), aiming at (1) confirming the *GC* as a positional candidate gene and (2) identifying a candidate causal variant.
90 This 10-Mb window contained the previously reported CNV, which was in high LD with the GWAS lead SNP [13]. Thus, we
91 kept SNPs located within the CNV in the WGS imputation panel, as they could possibly tag the CNV. The association signal
92 peaked in a 200-Kb region (BTA 6:88.5–88.7 Mb), spanning over *GC* and the region downstream of *GC*. The lead SNP,
93 rs110813063, located at BTA 6:88,683,517 ($-\log_{10}P=9.59$) was ~4 kb downstream of *GC* (Fig 1B). The T allele of the lead SNP
94 (allele frequency (AF) = 0.58), was associated with low CM resistance, whereas the C allele was associated with high CM
95 resistance (AF=0.42). Finally, a conditional analysis was performed by including the lead SNP as a covariate in the GWAS
96 model. SNPs in the association peak were no longer significant, with the exception of a minor signal at the left side of the
97 association peak (Fig 1C). Our results confirmed the presence of the CM resistance QTL in the Dutch HF population, however,
98 as with previous studies [7,13–15], the non-coding lead SNP (rs110813063) did not have any evidence of functional role.
99 There were no coding variants amongst the variant in high LD with the lead SNP ($r^2>0.9$). Provided that the strong association
100 signals do not necessarily indicate causality, due to confounding factors including LD and limited sample sizes [30], we further
101 characterized the lead SNP using WGS data.

102

103 A multi-allelic CNV is in high LD with the GWAS lead SNP for CM resistance QTL on BTA 6

104 By manually inspecting the WGS data, we observed that the GWAS lead SNP (rs110813063) was located within a ~12 kb CNV
105 encompassing the 14th exon of *GC* (Fig 2A). This CNV, present in both dairy and beef cattle populations [31], was reported to
106 be in high LD with the candidate SNP for CM resistance QTL in a Norwegian Red population [13]. Thus, we hypothesized that

107 the CNV might be the causal variant underlying this QTL. To confirm this hypothesis, we characterized the CNV using WGS
108 data of 266 HF animals. Our CNV calling pipeline, exploiting split-read, pair-end mapping, and read depth evidence, confirmed
109 the presence of the ~12 kb CNV at BTA 6:88,681,767-88,693,553 (hereafter referred to as GC CNV; S2 Fig). The 14th exon of
110 *GC*, encompassed by the CNV, is a 3' alternative exon, only accounting for minority of the total *GC* expression [13]. Sequenced
111 individuals presented either normal read depth (no CNV) or a highly inflated coverage, 2.5 to 5 times higher than expected
112 (CNV carriers; Fig 2B), implying multiple copies. To characterize whether different copy numbers (CN) were present at the GC
113 CNV locus, sequencing read depth information was used to obtain CN per individual (diploid CN). The distribution of this
114 diploid CN in the sequenced population suggested segregation of four different alleles corresponding to haploid CNs 1, 4, 5,
115 or 6 copies (Fig 2C). Based on these alleles and observed individual CN, we determined corresponding CN genotypes (e.g.,
116 individuals with CN 2 and 6 would be respectively carriers of alleles CN1/CN1 and CN1/CN5). The genotypes remained
117 ambiguous only for individuals with 10 copies, that could be either CN4/CN6 or CN5/CN5. In all sequenced duos or trios, these
118 inferred genotypes were compatible with Mendelian segregation rules (Fig 2D), and no genotype incompatibility was
119 observed. Genotypes from relatives of individuals with 10 copies allowed us also to deduce that all carriers of 10 copies were
120 CN4/CN6. Overall, these results suggest that the four alleles (CNs 1, 4, 5, and 6) are truly segregating in the population, rather
121 than the result of noise associated with depth estimation. Carriers of alleles CN5 or CN6 were restricted to a limited number
122 of families. In these families, the segregation of these two alleles perfectly matched haplotype transmission from parents to
123 offspring (S3 Fig), further supporting the presence of multiple alleles. An analysis of homozygosity-by-descent (HBD) in all
124 sequenced individuals revealed that alleles CN 4, 5 and 6 share a common haplotype, identical-by-descent for at least 200 kb
125 (≥ 600 SNPs; S1 Table). The HBD segments were rare at the CNV position in CN 1 individuals, presenting more haplotypic
126 diversity. Only two out of 88 heterozygous individuals were IBD in the studied position for an extremely short segment (12
127 kb, 93 SNPs), indicating that the CN 1 allele was associated with different haplotypes. In summary, we identified four alleles
128 at the GC CNV locus: CN 1 corresponds to a single copy and considered wildtype (Wt) given the high haplotypic diversity,
129 whereas alleles CNs 4-6 correspond to multiple copies (Mul), with four to six copies (Fig 3A). In our population, CN 1 and CN
130 4 were the most frequent alleles (0.39 and 0.54, respectively), while CN 5 and CN 6 were rare (0.03 and 0.05, respectively;
131 Fig 3A). Furthermore, the GC CNV, coded as a biallelic variant where CN 1 (Wt) was the reference allele and CNs 4-6 (Mul)
132 were grouped together as the alternative allele, was in perfect linkage ($r^2=1$) with the GWAS lead SNP (rs110813063). The T
133 allele, associated with low CM resistance, tagged CNs 4-6, whereas the C allele tagged CN 1. Thus, this SNP was used as a
134 surrogate marker for GC CNV in subsequent analyses. The GC CNV contained five tagging SNPs, including the GWAS lead SNP
135 ($r^2 \geq 0.98$; Fig 3B). These five tagging SNPs showed an allelic imbalance pattern in WGS data of Wt/Mul individuals (Fig 3C),
136 due to a disproportionately high number of reads, supporting alternative alleles on the duplication haplotypes. There was no
137 SNP uniquely tagging CNs 4-6 separately, due to their similar and recent haplotypic background.

138

139 **Recent positive selection strongly favoured a haplotype harbouring the GC CNV**

140 In livestock breeding, artificial selection for economically important traits (i.e. high CM resistance) potentially drives desired
141 alleles to fixation and removes alleles with negative effects (i.e. low CM resistance) from the population. Thus, it is intriguing
142 that the allele associated with low CM resistance (CNs 4-6) is highly frequent in Dutch HF cattle (combined AF=0.58). We
143 postulated two alternative hypotheses: (1) GC CNV is pleiotropic, conferring positive effects on different traits under selection,
144 contrary to a negative effect on CM resistance, or (2) GC CNV is in high LD with a causal variant of a strongly selected trait,
145 and therefore, genetic hitch-hiking increased the frequency of the low CM resistance allele. In both cases, the GC CNV would
146 be associated with a selected haplotype. Thus, BTA 6 was scanned for signatures of selection based on integrated Haplotype
147 Score (iHS [32,33]), using WGS haplotypes from the 266 HF animals. Of the two strong signals of selection identified near the
148 79 and 89 Mb regions (-log₁₀P>5; S4 Fig), the latter was only ~200 kb away from the GC CNV, and thus was further inspected
149 (Fig 4A). The extended haplotype homozygosity (EHH), centered at the iHS lead SNP (BTA 6:88,861,709, AF=0.28) revealed a
150 strongly favoured haplotype, which extended outwards further than the non-selected haplotypes (Fig 4B). As expected, CNs
151 4-6 were located in the strongly selected haplotype, whereas CN 1 was in the non-selected haplotypes. In addition, this finding
152 was in line with our HBD results, where homozygous CNV carriers (CNs 4-6) shared long HBD haplotypes, whereas
153 homozygous non-CNV carriers (CN 1) did not. These findings supported our hypothesis that a strong positive selection acted
154 upon the region containing the GC CNV. Given the antagonistic effects of the CM resistance QTL on MY [13] and relevance to
155 dairy cattle breeding [34], we deemed MY as a potential target of the selection signature we identified. To confirm whether
156 CM resistance and MY are modulated by the same variant (pleiotropy) or two different variants (LD), the 10-Mb window (BTA
157 6:84-93 Mb) harbouring the GC CNV was fine-mapped for MY. A strong association signal appeared in 89.08 Mb region, ~400
158 kb away from the GC CNV (-log₁₀P=7.5; Fig 4A). The lead SNP was found at 89,077,838-bp and the G allele was associated
159 with high MY, whereas the T allele was associated with low MY (AF=0.45). Regardless of the ~400-Kb distance, the MY lead
160 SNP and the GC CNV were in high LD ($r^2 = 0.88$). Of note, the iHS lead SNP was located between the association signals for CM
161 resistance and MY (Fig 4A). We re-evaluated the EHH results and found that the strongly selected haplotype harbours CNs
162 4-6 alleles of the GC CNV and the G allele of the MY lead SNP, implying that the strong selection resulted in low CM resistance
163 and high MY (Fig 4B). We sought to disentangle these two QTL further, to elucidate whether they are in LD or pleiotropy.
164 However, due to a high LD and limitation in the data set (only 13 out of ~4,000 bulls carrying favourable recombinant
165 haplotypes), this was not possible with the current data.
166 Additionally, we fine-mapped other dairy cattle traits, in an attempt to identify other potential selection target trait(s). Our
167 results showed that the GC CNV was the lead variant for body condition score (BCS) and calving interval (CI; -log₁₀P=21.4 and
168 6.6, respectively). Notably, GC CNV had a stronger association signal for BCS than it did for MY (S5 Fig). The CNs 4-6 allele,

169 which was associated with low CM resistance, was correlated with low BCS (meaning low body fat content) and longer CI
170 (meaning low fertility). The SNP association p-values obtained from either CM resistance and BCS or CM resistance and CI,
171 clearly colocalized, underlining that these QTL are driven by the same variant, which is likely to exert pleiotropic effects on
172 each of these traits (S4 Fig and S2 Table).

173

174 **GC is the most functionally relevant gene underlying the CM resistance QTL on BTA 6**

175 Our GWAS results hinted at transcriptional regulation as an underlying mechanism(s) of the CM resistance QTL, as our GWAS
176 lead SNP was found in non-coding region. Thus, we mapped *cis*-expression QTL (further referred to as eQTL), to (1) identify
177 shared variant(s) that are driving both GWAS and eQTL signals, and (2) to corroborate the causality of the candidate gene *GC*
178 in the major CM resistance QTL. Prior to eQTL mapping, we firstly determined the most biologically relevant tissue(s) for our
179 investigation. In the human transcriptome database [35–40], *GC* is predominantly expressed in the liver, whereas breast
180 tissue showed no expression (S3 Table). Also, previous dairy cattle transcriptome studies showed that *GC* is expressed in the
181 liver, kidney, and cortex, but not in the mammary gland [12,13,41]. Therefore, we performed eQTL mapping within the *cis*-
182 regulatory range (+/- 1Mb region from the *GC* CNV), using liver RNA-seq data and Bovine HD genotype of lactating HF cows
183 (n=175). Since *GC* CNV is not in the BovineHD array, the *GC* CNV genotypes were obtained by (1) imputing BovineHD
184 genotypes to WGS level variants and (2) genotyping the *GC* CNV directly. Direct genotyping was done by targeting six
185 polymorphic sites (CN 1 as reference allele and CNs 4-6 as alternative allele) in the *GC* CNV (S4 Table). The best probe
186 (BTA6:88,683,517) among the six showed 100% compatibility with the imputed *GC* CNV genotypes, underlining that our
187 imputation approach was robust. Hence, we used the imputed genotypes (BTA6:87-89 Mb) to map eQTL further. The RNA-
188 seq data was mapped using a reference guided method, where both reference annotated transcripts and novel transcripts
189 can be discovered. Our RNA-seq data detected two different *GC* transcript isoforms: a canonical and an alternative transcript
190 (Fig 5A). The former consisted of 13 exons and accounted for a majority of overall *GC* expression (~98%). The latter shared
191 the first 12 exons with the canonical transcript, however, it used an alternative 3' exon, the 14th exon, which is located inside
192 the *GC* CNV. Expression of the alternative transcript was relatively low (~2% of the total *GC* expression). The reference gene
193 set used for transcript assembly included the canonical form, but not the alternative transcript. Thus, *GC* gene-level eQTL
194 mapping was done on the canonical form, and we additionally mapped transcript-level eQTL for the alternative *GC* transcript.
195 Of the 13 genes annotated within the *cis*-regulatory range of CNV (+/- 1 Mb), *GC* was abundantly expressed ($\geq 5,000$
196 transcripts per million (TPM)) and other genes were either lowly expressed ($0.1 < \text{TPM} < 50$), or not expressed (Fig 5B). Our
197 gene-level eQTL mapping results discovered highly significant *cis*-eQTL for *GC* and *SLC4A4*. The *GC* *cis*-eQTL was found in the
198 BTA 6:88.68-88.89 Mb region ($-\log_{10}P > 23$; Fig 5D). The *GC* CNV was one of the top variants within the eQTL peak ($-\log_{10}P=24.4$)
199 and was in high LD with the *GC* eQTL lead SNP ($-\log_{10}P=25.4$; $r^2=0.88$). P-values for *GC* expression and CM resistance were

200 highly correlated ($p=0.68$; Fig 5E), where CNs 4-6 were associated with increased *GC* expression and low CM resistance (Fig
201 5F). The *SLC4A4* *cis*-eQTL was found in BTA 6:88.67-89.07 Mb ($-\log_{10}P > 7$, S6 Fig). The lead SNP for *SLC4A4* eQTL (BTA
202 6:88,672,979, $-\log_{10}P=7.75$) was found ~9 kb away from *GC* CNV, which also showed high significance ($-\log_{10}P=7.1$). The *GC*
203 CNV and the lead SNP for *SLC4A4* eQTL were in high LD with *GC* CNV ($r^2=0.99$). P-values obtained from *SLC4A4* eQTL mapping
204 and CM resistance were highly correlated ($p=0.82$), and CNs 4-6 were associated with increased *SLC4A4* expression (S6 Fig).
205 Additionally, we detected a transcript-level eQTL for the alternative *GC* transcript. Intriguingly, the eQTL signal was driven by
206 *GC* CNV tagging SNPs, followed by the second most significant variant, *GC* CNV ($-\log_{10}P=16.9$ and 16.4, respectively; Fig 5G).
207 P-values for alternative *GC* transcript expression and CM resistance were correlated even stronger than the canonical
208 transcript ($p=0.74$; Fig 5H), where CNs 4-6 corresponded to an increased expression of the alternative *GC* transcript (Fig 5F).
209 Our results indicate *GC* as a promising candidate gene, given the strong eQTL signal. On the contrary, high LD between *GC*
210 CNV and the *SLC4A4* eQTL lead SNP ($r^2 =0.99$), implied that *SLC4A4* could be a candidate gene. To prioritize between the two
211 candidate genes *GC* and *SLC4A4*, we used summary data-based Mendelian randomization (SMR) analysis [42], which
212 estimates associations between phenotype and gene expression, aiming at identifying a functionally relevant gene,
213 underlying GWAS hits. Our result showed *GC* to be the only gene whose expression was significantly associated with CM
214 resistance association ($-\log_{10}P=6$), whereas *SLC4A4* was below the statistical threshold ($-\log_{10}P=4.9$; S5 Table). A subsequent
215 analysis, heterogeneity in dependent instruments (HEIDI), was conducted to test whether the significant association between
216 GWAS hit and eQTL shown for *GC* was induced by a single underlying variant or two variants that are in LD (i.e. GWAS hit
217 variant is in LD with eQTL lead SNP). The result suggested a single underlying variant modulating both CM resistance GWAS
218 and *GC* eQTL ($P_{HEIDI} = 0.06$). Thus, we confirmed *GC* as the most promising causal gene underlying CM resistance QTL, whose
219 expression affects the CM resistance phenotype.

220

221 **A putative enhancer located in the *GC* CNV likely modulates the level of *GC* expression**

222 We subsequently exploited epigenomic data sets to infer the functions of candidate variants in the 200-kb *GC* eQTL region
223 (BTA 6:88.68-88.89 Mb; Fig 6A). Bovine liver epigenomic data, interrogating two histone modifications (ChIP-seq for H3K27ac
224 and H3K4me3 marks) [43] and open chromatin regions (ATAC-seq) [manuscript in preparation] were investigated to infer
225 functional contexts (i.e. active promoters and enhancers). The ChIP-seq data predicted one active promoter and three active
226 enhancers, overlapping with ATAC-seq peaks, supporting the active status of the regulatory elements along *GC* (Fig 6A). Of
227 the three putative enhancers identified, *GC* harbours two putative enhancers: one located inside the *GC* CNV (further referred
228 to as *GC* CNV enhancer), and could be considered highly active, given the strong H3K27 acetylation mark. According to the
229 comparative genomics catalogue of regulatory elements in liver [43], the *GC* CNV enhancer is cattle-specific, whereas the
230 intronic enhancer is conserved between human, mouse, cow, and dog. These two putative enhancers were both supported

231 by corresponding ATAC-seq signals, with a stronger peaks for the GC CNV enhancer (Fig 6A). Additionally, this strong ATAC
232 signal overlapped with a repetitive element, MER115, from the DNA transposon family, hAT-Tip100 (Fig 6B). Some DNA
233 transposons obtain enhancer function during evolution [44], and hAT-Tip100 was shown to function as enhancer in humans
234 [43]. However, although the human orthologous region harbours MER115, this repeat did not show enhancer activity in
235 humans [40], underlining cattle-specific enhancer activity. Finally, we scanned the ATAC peak region inside the GC CNV,
236 searching for transcription factor binding (TFB) motifs using Homer [45]. We found strong evidence for five motifs, including
237 transcriptional enhancer factor (*TEAD*) and hepatocyte nuclear factor 4 alpha (*HNF4A*), supporting for the presence of the
238 active enhancer within the GC CNV (Fig 6C).

239

240

241 **Discussion**

242 In this study, we dissected a prominent CM resistance QTL in Dutch HF cattle, by integrating GWAS, eQTL, and functional
243 (epi)genomics data. Our findings revealed that the GWAS lead variant is the GC CNV, a 12-kb multi-allelic CNV, which harbours
244 a putative *cis*-regulatory element which targets *GC*. This CNV drives both the CM resistance association and the *GC* eQTL
245 signals, underscoring *GC* as the likely causal gene underlying this QTL.

246 Identifying causal variants from GWAS can be challenging, since, often non-causal SNPs in high LD with the causal variant
247 appear as lead SNPs [30]. Notably, our GWAS candidate SNP (rs110813063) has not been considered a strong candidate in
248 other fine-mapping studies [7,13,14]. The function of our lead SNP, located 4-kb downstream of *GC*, was equally elusive,
249 compared to other candidate SNPs that were located in the intronic region of or upstream of *GC* [7,13–15]. Nonetheless, the
250 allelic imbalance pattern in our candidate SNP (Fig 3C), together with a previous report about a CNV in high LD with the GWAS
251 candidate SNP [13], motivated us to speculate that the CNV might be the causal variant. As expected, we corroborated that
252 our GWAS lead SNP, rs110813063, is a perfect tag SNP of the GC CNV ($r^2=1$). There are several explanations why previous
253 fine-mapping studies missed rs110813063. Possibly, this SNP was absent in the GWAS variant set, as the standard SNP quality
254 control (QC) criteria (i.e. removing SNPs with high depth and/or unbalanced allelic ratio) tend to eliminate SNPs inside CNVs.
255 Alternatively, rs110813063 was present, but wrongly genotyped, due to highly disproportional allelic depth (Fig 3C). Hence,
256 one may wonder whether a SNP-based GWAS approach, relying on a stringent QC, is sufficient in identifying causal variants,
257 in a form other than point mutations. The answer might depend on the type of variant: studies showed that most deletions
258 are well captured by tagging SNPs, whereas most duplications and multi-allelic CNVs are poorly tagged [46,47]. Thus, an
259 exploratory check for presence of CNVs might be beneficial for fine-mapping studies.

260 To connect the discovery from statistical associations to the molecular function, we showed that the association mapping
261 signal was driven by the underlying molecular signal, expression of *GC* (Fig 5). Many heritable diseases are manifested in a
262 tissue-specific manner [48]. Our trait of interest, CM, is manifested in the mammary glands, and hence it was considered a
263 biologically relevant tissue for eQTL mapping. However, both large-scale human transcriptome databases (S2 Table) and
264 cattle transcriptome studies indicated liver as the main organ of *GC* expression [1–3]. This discrepancy shows that prior
265 knowledge of tissue-specific manifestation of a trait is crucial for elucidating its molecular basis. In cattle, eQTL data was
266 generated from diverse tissues (adrenal gland, blood, liver, mammary gland, milk, and muscle) [49–55], and some studies
267 utilized the data sets in confirming causality of candidate genes [49–51,53]. We expect that the availability of eQTL data sets
268 of diverse tissues and cell types will lead to rapid discovery and confirmation of candidate genes in farm animals in the future.
269 Bovine epigenomic data sets were utilized to prioritize candidate variants for the CM resistance QTL and eQTL for *GC*
270 expression. The ChIP-seq and ATAC-seq data supported three active enhancers and one active promoter in the region of
271 interest (Fig 6A). Of these regulatory elements, the *GC* CNV enhancer is considered the most likely causal variant, as multiple

272 copies of enhancers can increase the target gene expression [56]. Hence, we propose that altered *GC* expression, mediated
273 via multiplicated enhancers, is likely the key regulatory mechanism for this QTL. Interestingly, candidate causal variants
274 reported by previous studies [13,14] were found in the 1st intron of or upstream of *GC*, where an active enhancer and an
275 active promoter were found (Fig 6A). In humans, tissue-specific enhancers outnumber protein coding genes [40,57]. Hence,
276 a gene can be regulated by more than one enhancer, and a secondary enhancer is referred to as a shadow enhancer [58]. A
277 recent study showed that redundant enhancers function in an additive manner, thus conferring phenotypic robustness (e.g.
278 activities of multiple enhancers act together, thus removal of an enhancer still results in discernible phenotypes) [59]. In light
279 of this finding, we speculate that the two enhancers located in *GC*, might have additive effects on *GC* expression.
280 Mammalian enhancers evolve rapidly, compared to promoters [43]. Also, rapidly evolving enhancers were exapted from
281 ancestral DNA sequences and associated with positively selected genes [43]. The *GC* CNV enhancer is likely one of these
282 rapidly evolving enhancers, given that (1) it exapted MER115, which does not function as enhancer in other species, (2) it is
283 found in a selective sweep which harbors *GC*, and (3) it is cattle-specific. These findings strongly suggest that utilizing
284 epigenomic data of species other than the one of interest, can be misleading, as it lacks species-specific regulatory elements.
285 This provides a compelling reason to build species-specific epigenome maps, as already embarked upon by the international
286 Functional Annotation of Animal Genomes (FAANG) project [60,61]. With this community effort, a wider range of species-
287 specific regulatory elements underlying economically important QTL is expected to be unraveled in the future.
288 The major CM resistance QTL is known to have antagonistic effects for MY [13,14] and our results confirmed this. The trade-
289 off between CM resistance and MY suggests that this locus might be under balancing selection [62]. One of the drivers of
290 balancing selection is strong directional selection, which is common in livestock breeding [63]. Of the two traits of interest,
291 MY has been the primary goal of dairy cattle breeding [34], and hence it seems plausible to assume that this locus is under
292 balancing selection. Next to this, we had a particular interest in understanding the genetic basis of the antagonistic effects.
293 The genetic modes considered were (1) a single pleiotropic variant affecting two traits and (2) two independent causal
294 variants for each trait, in high LD. In case of pleiotropy, a particular genomic region cannot enhance both traits simultaneously
295 through breeding. However, in case of LD, selection for recombinant haplotypes, containing favourable alleles for both traits,
296 enables simultaneous improvement on the two traits. Only a small number (0.3%) of the studied animals had recombinant
297 haplotypes (13 out of 4,142 bulls), and hence our data set lacks sufficient power to distinguish LD from pleiotropy. Future
298 studies might consider two approaches for discerning this issue. The first is to exploit a daughter design by obtaining sufficient
299 daughters of the 13 recombinant haplotype carrier Dutch HF bulls [64]. Another possibility would be to harness data from
300 different breed(s). A dairy cattle breed that has both MY and CM resistance recorded, yet with low LD in the QTL region,
301 would be most useful. Otherwise, a meta-GWAS of multiple cattle populations can aid in distinguishing between LD and
302 pleiotropy.

303 We attempted to integrate the findings from the current study and further speculate on how *GC* expression and CM resistance
304 are linked, assuming that the level of *GC* expression and DBP is correlated; meaning absence of post-transcriptional
305 /translational regulation (Fig 7). DBP binds to and transports vitamin D [65], yet it plays additional roles in bone development,
306 fatty acid transport, actin scavenging, and modulating inflammatory responses (see [23,66] for review). To start with, DBP
307 modulates immunity as a macrophage activating factor (DBP-MAF), when deglycosylated via glycosidases of T- and B- cells
308 [67,68] and therefore enhances the immune response. Accordingly, we could hypothesize that CNV carriers have larger
309 amounts of DBP, and subsequently improved immunity, leading to higher CM resistance. However, this hypothesis contradicts
310 with our findings, as CNV carriers were shown to have lower CM resistance. Alternatively, DBP regulates the amount of freely
311 circulating vitamin D metabolites [69]. According to the free hormone hypothesis, only free vitamin D metabolites are able
312 to cross the cell membrane, and are thus biologically available [70]. In humans, only 0.03 % of 25(OH)D, an indicator of vitamin
313 D, is free, whereas the majority of vitamin D is bound either to DBP (85%) or to albumin (15%) [69]. Under these circumstances,
314 CNV carriers, having a large pool of DBP, can be hypothesized to have lower levels of biologically available vitamin D, as
315 postulated in human studies [71,72]. Thus, presumably, if CNV carriers have low amounts of free vitamin D, which may be
316 termed as 'vitamin D deficiency', low CM resistance in these animals seems like a logical consequence (Fig 7).

317 Although vitamin D has been considered crucial in bone health [24], a recent review showed an inverse correlation between
318 vitamin D concentrations and an extensive range of ill-health outcomes in humans [73]. Given the pervasive association
319 between vitamin D and health conditions, there may be other associated traits induced by vitamin D deficiency. Indeed, we
320 found strong association signals for BCS and CI, exerted by the GC CNV, implying its pleiotropic effects for multiple traits (S5
321 Fig). The CNs 4-6, which were associated with low CM resistance, were associated with longer CI, meaning poor fertility. CI, a
322 measure of duration from one calving to the next, is an indicator of fertility issues such as perturbations in the oestrous cycle,
323 and/or anovulation [74]. Human studies reported ovarian dysfunction induced by vitamin D deficiency [75]. This finding
324 provides convincing evidence that the GC CNV might be the underlying variant inducing vitamin D deficiency and suboptimal
325 female fertility. Furthermore, pleiotropic effects of the GC CNV indicated that CNs 4-6 were associated with low CM resistance
326 and low BCS. This finding fits with the results found in HF cattle where low BCS was genetically correlated with high disease
327 incidence [76], although the causal relationship between CM resistance and BCS remains unknown. Intriguingly, human
328 studies showed contradictory results: obesity, a condition analogous to high BCS, predisposes patients to vitamin D deficiency,
329 leading to disease susceptibility [51]. These opposing consequences of body composition traits possibly hint at an 'optimum'
330 body fat amount, where an organism can function well without compromising its health.

331 **Conclusions**

332 In this study, we dissected the major CM resistance QTL on BTA 6, integrating GWAS, CNV calling, eQTL mapping, and
333 functional prioritization of candidate variants. We revealed a multi-allelic CNV harbouring a strong enhancer targeting *GC*, as

334 the likely causative variant. Our findings revealed that the candidate causal gene *GC* is likely regulated by an enhancer located
335 in the *GC* CNV. We speculate that *GC* CNV carriers which were shown to have high *GC* expression would have a larger amount
336 of *DBP*, and by extension low amount of biologically available vitamin D. This physiological condition probably puts animals
337 into a state analogous to vitamin D deficiency and leads to low CM resistance. Moreover, we report evidence of pleiotropic
338 effects of the *GC* CNV for other economically important traits as *BCS*, *CI*, and *MY*, which revolves around the vitamin D
339 pathway. The current study provides a novel example of multiplicated *cis*-regulatory elements playing pleiotropic roles on
340 various polygenic traits in dairy cattle.

341

342

343 **Materials and methods**

344 **Whole genome sequencing and variant discovery**

345 **Whole genome sequence data**

346 The genomes of 266 Dutch HF animals were sequenced. These 266 animals were closely related animals, where 240 were
347 forming parents-offspring trios. The biological materials were either from sperm (males) or whole blood (females and males).
348 Whole genome Illumina Nextera PCR free libraries were constructed (550bp insert size) following the protocols provided by
349 the manufacturer. Illumina HiSeq 2000 instrument was used for sequencing, with a paired end protocol (2x100bp) by the
350 GIGA Genomics platform (University of Liège). The data was aligned using BWA mem (version 0.7.9a-r786) [77] to the bovine
351 reference genome UMD3.1 , and converted into bam files using SAMtools 1.9 [78]. Subsequently, the bam files were sorted
352 and PCR duplicates were marked with Sambamba (version 0.4.6) [79]. All samples had minimum mean sequencing depth of
353 15X and the mean coverage of the bam files was 26X.

354 **SNP calling and imputation panel construction**

355 Variant calling was done using GATK Haplotype caller in N+1 mode. We applied Variant Quality Score Recalibration (VQSR) at
356 truth sensitivity filter level of 97.5 to remove spurious variants. Using the trusted SNP and indel data sets which are explained
357 elsewhere [80], we observed that the VQSR step filtered out GC CNV tagging SNPs, possibly due to the overwhelmingly high
358 depth in this region. Yet, GC CNV tagging SNPs were considered crucial in our research, as we considered that they could tag
359 the GC CNV. Therefore, the genotypes of the GC CNV tagging SNPs obtained from the raw variant calling format (VCF) file
360 were inserted in the VQSR filtered VCF file. While inspecting the CNV tagging SNPs, we discovered genotyping errors (three
361 errors among 5 tagging SNPs of 266 individuals), where Ref/Alt was wrongly genotyped as Alt/Alt, due to severe allelic
362 imbalance (where the number of alternative allele supporting reads is predominantly high). Using parent-offspring
363 relationships available in our data set, we confirmed that these were true errors, and hence they were manually corrected.
364 Finally, the VCF file of sequence level variants in BTA 6:84-94Mb, containing manually corrected GC CNV tagging SNPs was
365 obtained. This VCF file, consisting of 45,820 variants of 266 animals was used as an imputation panel for fine-mapping
366 analyses. For analyses related to haplotype segregation among the 266 sequenced animals, haplotype sharing among carriers
367 and identification of selection signatures, we further applied stringent variant filters on the VCF file as explained in [81] to
368 conserve only highly confident variants and to remove spurious genotyping and map errors.

369 **Genome-wide association studies**

370 **Phenotype and genotype data**

371 We obtained genotype and phenotypic data of 4,142 progeny tested HF bulls from Dutch HF cattle breeding programme (CRV
372 B.V., Arnhem, the Netherlands). The phenotype data was consisting of 60 traits, which are routinely collected in the breeding

373 programme, including clinical mastitis resistance (S6 Table). The estimated breeding values (EBVs) were de-regressed to
374 correct for the contribution of family members and de-regressed EBVs were used as phenotypes in GWAS. The effective
375 daughter contributions of the 4,142 bulls for CM resistance ranged between 25 and 971.3, with an average of 204.3. The
376 4,142 bulls were genotyped with a low density genotyping array (16K). Afterwards, the 16K genotype data was imputed in
377 two steps, firstly to 50K density, based on two private versions of a Bovine 50K genotyping array, and the panel was consisting
378 of 1,964 HF animals. It was further imputed to a higher density, using a panel of 1,347 HF animals genotyped with Illumina
379 BovineHD BeadChip (770K). Subsequently, the data was imputed to sequence level using the HF WGS imputation panel
380 described above. The imputation was done with Beagle 4 [82], and variants with low minor allele frequency (MAF < 0.025)
381 and low imputation accuracy (allele R² < 0.9) were filtered out.

382 **Association model and conditional analysis**

383 To confirm the presence of CM resistance QTL on BTA 6 in the Dutch HF population, we performed association mapping using
384 imputed high density genotypes (BovineHD (770K) reference panel). The association mapping was performed SNP-by-SNP
385 with a linear mixed model in GCTA [83]. The following model was fitted :

386
$$\mathbf{y} = \mathbf{1}\boldsymbol{\mu} + \mathbf{X}\mathbf{b} + \mathbf{g} + \mathbf{e}$$

387 where \mathbf{y} is the vector of phenotypes (de-regressed EBVs), $\mathbf{1}$ is a vector of ones, $\boldsymbol{\mu}$ is the overall mean, \mathbf{X} is a vector of SNP
388 genotypes coded as biallelic variant (0, 1, or 2), \mathbf{b} is the additive effect of the SNP which is being tested for association, \mathbf{g} is
389 the polygenic effect captured by a genomic relationship matrix (GRM; random effect), and \mathbf{e} is the residual. The GRM was
390 built with GCTA, based on 50K genotypes to avoid losing statistical power by including causal markers [84]. The model
391 assumed equal residual variances. A SNP was regarded significantly associated with CM, when -log₁₀P value was above 6.45
392 (chromosome-wide Bonferroni multiple-testing correction for 28,669 tests), at a nominal significance of p = 0.01.
393 Subsequently, we repeated the association analysis in the BTA 6:84-94 Mb region, using the imputed sequence level variants
394 (n=45,820) to fine-map the QTL. The association model used was same as described above. Finally, to test if the lead SNP
395 explained the QTL signal completely we ran a conditional association analysis for the imputed sequence variants in BTA 6:84-
396 94 Mb region with the lead SNP as a covariate in the model.

397 **CNV discovery and characterization of GC CNV**

398 The CNV was called from the WGS data of 266 animals, using the Smoove pipeline (<https://github.com/brentp/smoove>). This
399 pipeline collects split and discordant reads using Samblaster [85], and then calls CNVs using Lumpy [86]. Afterwards, the CNV
400 sites were genotyped using SVTyper (<https://github.com/hall-lab/svtyper>). Additionally, we used Duphold [87] to calculate
401 read depth of the CNs at the GC CNV locus. Duphold exploits read depth between copy number variable regions and normal
402 regions and calculates the ratio between these two. The integer diploid CNs obtained based on the Duphold coverage ratio
403 values were assigned to the 266 animals. The CN distribution showed peaks at diploid CNs of 2, and 5-10, implying four

404 haploid CNs (1, 4, 5, and 6) segregating at the GC CNV locus. Thus, possible haplotypic combinations for the diploid CNs would
405 be: 2 (1/1), 5 (1/4), 6 (1/5), 7 (1/6), 8 (4/4), 9 (4/5), 10 (4/6 or 5/5). There was only one haplotypic combination possible for
406 all the diploid CNs, except 10, were either (4/6) or (5/5) could form diploid CN 10. We confirmed the true presence of these
407 CN alleles by taking advantage of our family structure. First, we verified that observed genotyped followed the Mendelian
408 segregation rules. Next, we also checked that CN alleles transmission within the pedigree was in agreement with haplotype
409 transmission. Haplotypes were reconstructed using familial information and linkage information using LINKPHASE3
410 programme [88]. The program estimates also, at each marker position and for each parent-offspring pair, the probability that
411 a progeny inherited the paternal or the maternal haplotype for its parents.

412 To study the relationship between different CN alleles, we estimated homozygous-by-descent (HBD) probabilities at the CNV
413 locus, and measured length of identified HBD segments. To that end, we ran with RZooRoH [89] a multiple HBD-class model
414 described in [90], with four HBD classes and one non-HBD class with rates equal to 10, 100, 1000, 10,000 and 10,000,
415 respectively. As this approach compares haplotypes within individuals, it does not require haplotype reconstruction and is
416 not affected by eventual phasing errors.

417 **Selection signature analyses**

418 The BTA 6 was scanned for haplotype based selection signatures observed in the sequence variants from the 266 animals.
419 We used the integrated haplotype homozygosity score (iHS [33]) using 'rehh' R package [32] for within-population analysis of
420 recent selection signatures. In order to unravel the selection target trait(s) we identified a number of traits within the
421 routinely collected catalogue of 60 traits showing QTL signals in the 84-94Mb region on BTA 6 based on 16K GWAS results
422 (EuroGenomics custom SNP chip [91]). Hence, we performed GWAS for these traits (BCS, CI, and MY) in BTA 6:84-94Mb region
423 based on imputed WGS variants to fine-map those QTL. The input files and the association model for the GWASs were the
424 same as described above, except that phenotypes used de-regressed EBVs of BCS, CI, and MY, respectively. The GWAS results
425 of these traits were plotted against the GWAS result of CM resistance to characterize the colocalization of QTL signals, using
426 the R package "LocusComparer" [92].

427 **eQTL mapping and Summary data-based Mendelian randomization analysis**

428 **RNA-seq data and eQTL mapping**

429 We used RNA-seq data produced by the GplusE consortium (<http://www.gpluse.eu/>; EBI ArrayExpress: E-MTAB-9348 and
430 9871)(Wathes et al; accepted but not online yet). Briefly, liver biopsy samples were collected from ~14 day post-partum HF
431 cows (n=178). The procedures had local ethical approval and complied with the relevant national and EU legislation under
432 the European Union Regulations 2012 (S.I. No. 543 of 2012). RNA-seq libraries were constructed using Illumina TruSeq
433 Stranded Total RNA Library Prep Ribo-Zero Gold kit (Illumina, San Diego, CA) and sequenced on Illumina NextSeq 500
434 sequencer with 75-nucleotide single-end reads to reach average 32 million reads per sample. The reads were aligned to the

435 bovine reference genome UMD3.1 and its corresponding gene coordinates from UCSC as a reference using HISAT2 [93].
436 Transcript assembly was conducted with StringTie [94], using reference-guided option for transcript assembly, which enables
437 discovery of novel transcripts that are not present in the reference gene set. Reads were counted at gene- or transcript-level
438 using StringTie. After data normalization using DESeq2 [95], we performed principal component (PC) analyses and removed
439 outliers (PC > 3.5 standard deviations from the mean for the top four PCs, n=2). Subsequently, the gene expression levels
440 were corrected with Probabilistic Estimation of Expression Residuals (PEER) [96]. All animals were genotyped using Illumina
441 BovineHD Genotyping BeadChip (770K). The genotype data was imputed to WGS level, using the imputation panel explained
442 above, using Beagle 4 [82] and variants with low minor allele frequency (MAF < 0.025) and low imputation accuracy (allele R²
443 < 0.9) were filtered out. Finally, the PEER corrected normalized gene expression was associated with the imputed WGS
444 variants for 175 samples, using a linear model in R package “MatrixEQTL” [97].

445 **Prioritizing the causal gene**

446 We prioritized the most functionally relevant gene for the CM resistance QTL on BTA 6, using SMR (version 1.03) [42], to
447 estimate association between phenotype and gene expression. Input data required were summary statistics from CM
448 resistance GWAS and eQTL mapping results explained above. Additionally, the program requires plink format genotype data
449 to analyse LD in the region of interest, for which the imputed WGS variants (BTA 6:84-94 Mb) of 4,142 bulls were used. A
450 subsequent analysis, heterogeneity in dependent instruments (HEIDI), was conducted to test whether the significant
451 association between GWAS hit and eQTL shown for GC was induced by a single underlying variant or two variants that are in
452 LD (i.e. GWAS hit variant is in LD with eQTL lead SNP). The statistical thresholds for SMR (-log₁₀P>5) and HEIDI (P > 0.05) were
453 benchmarked from the original paper [42].

454 **Functional genomics assay data**

455 The human transcriptome data bases were examined to find out in which tissue GC is highly expressed via Ensembl website
456 (release 101; [98]). We downloaded liver ChIP-seq data (H3K27ac and H3K4me3) generated from four bulls from ArrayExpress
457 (E-MTAB-2633 [43]). This ChIP-seq data was aligned to the bovine reference genome UMD3.1 using Bowtie2 [42] and peaks
458 were called using MACS2 [99]. A catalogue of mammalian regulatory element conservation
459 (<https://www.ebi.ac.uk/research/flicek/publications/FOG15>) was used to infer the conservation of the regulatory elements
460 predicted from the ChIP-seq data sets. Next, ATAC-seq data was explored to see if chromatin accessible regions coincided
461 with the histone marks obtained from the ChIP-seq data. We obtained a male calf’s liver ATAC-seq data from the GplusE
462 consortium (ArrayExpress accession number: E-MTAB-9872). Data was analysed by following the ENCODE Kundaje lab ATAC-
463 seq pipeline (<https://www.encodeproject.org/pipelines/ENCP1792NWO/>). Sequences were trimmed using Trimmomatic [41]
464 and aligned on the bovine reference genome UMD3.1 using Bowtie2 [42]. After filtering out low quality, multiple mapped,
465 mitochondrial, and duplicated reads using SAMtools [43] and the Picard Toolkit (<http://broadinstitute.github.io/picard/>),

466 fragments with map length ≤ 146 bp were kept as nucleosome-free fraction. Genomic loci targeted by TDE1 were defined
467 as 38-bp regions centered either 4 (plus strand reads) or 5-bp (negative strand reads) downstream of the read's 5'-end. ATAC-
468 seq peaks were called using MACS2 [99] (narrowPeak with options --format BED, --nomodel, --keep-dup all, --qvalue 0.05, --
469 shift -19, --extsize 38). We inspected the presence of an enhancer in the human orthologous region of the GC CNV, using
470 ENCODE data [40] in the UCSC genome browser [100]. Transcription factor (TF) binding motifs in ATAC-seq peak regions were
471 discovered using Homer [45]. The TF motifs that are expressed in bovine or human liver are kept and shown in the figure
472 [101,102].

473

474 **EuroGenomics custom array genotyping**

475 We attempted to directly genotype the GC CNV in a biallelic mode (CN 1 as reference allele and CNs 4-6 as alternative allele).
476 Probes targeting six polymorphic sites were designed in Illumina DesignStudio Custom Assay Design Tool were added to
477 custom part of the EuroGenomics array [91] (S4 Table). DNA was extracted from the same biological material used for RNA-
478 seq used for eQTL mapping (described above), and genotyped for the EuroGenomics array by the GIGA Genomics platform
479 (University of Liège). The SNP genotypes were assessed using Illumina GenomeStudio software. Average call rate per probe
480 was calculated to assess the quality of the probes. Finally, genotypes obtained from the highest quality (BTA6:88,683,517)
481 was compared to the imputed GC CNV genotypes.

482

483 **Acknowledgements**

484 The Dutch HF whole genome sequence population data set was funded by the DAMONA ERC advanced grant to Michel
485 Georges. The authors are grateful to Elias Kaiser for discussion on the Vitamin D pathway, Ole Madsen for discussion on
486 functional genomics data, Martijn Derkx for providing advice on CNV calling pipeline, and the GplusE consortium for
487 providing data for eQTL mapping and ATAC-seq.

488

489 **Author contribution**

490 **Conceptualization:** Michel Georges, Carole Charlier, Aniek Bouwman

491 **Data Curation:** Wouter Coppieters, Latifa Karim, Gabriel Costa Monteiro Moreira, Haruko Takeda, Erik Mullaart, Ruth
492 Appeltant

493 **Formal analysis:** Young-Lim Lee, Tom Druet, Haruko Takeda

494 **Funding Acquisition:** Roel Veerkamp, Michel Georges

495 **Investigation:** Young-Lim Lee, Tom Druet, Haruko Takeda

496 **Methodology:** Aniek Bouwman, Tom Druet, Haruko Takeda
497 **Resources:** Erik Mullaart
498 **Supervision:** Carole Charlier, Mirte Bosse, Tom Druet, Aniek Bouwman, Michel Georges, Martien Groenen, Roel Veerkamp
499 **Visualization:** Young-Lim Lee
500 **Writing – original draft preparation:** Young-Lim Lee
501 **Writing – review & editing:** Young-Lim Lee, Carole Charlier, Mirte Bosse, Tom Druet, Aniek Bouwman, Michel Georges,
502 Martien Groenen, Roel Veerkamp, Wouter Coppieeters, Latifa Karim, Gabriel Costa Monteiro Moreira, Haruko Takeda, Erik
503 Mullaart, Ruth Appeltant
504
505

506 **References**

- 507 1. Halasa T, Huijps K, Østerås O, Hogeweine H. Economic effects of bovine mastitis and mastitis
508 management: A review. *Vet Q.* 2007;29(1):18–31.
- 509 2. Zwald NR, Weigel KA, Chang YM, Welper RD, Clay JS. Genetic Selection for Health Traits Using
510 Producer-Recorded Data . I . Incidence Rates , Heritability Estimates , and Sire Breeding Values. *J Dairy*
511 *Sci* [Internet]. 2004;87(12):4287–94. Available from: [http://dx.doi.org/10.3168/jds.S0022-0302\(04\)73573-0](http://dx.doi.org/10.3168/jds.S0022-0302(04)73573-0)
- 512 3. Bloemhof S, Jong G De, Haas Y De. Genetic parameters for clinical mastitis in the first three lactations
513 of Dutch Holstein cattle. *Vet Microbiol.* 2009;134:165–71.
- 514 4. Negussie E, Lidauer M, Nielsen US, Aamand GP. Combining Test Day SCS with Clinical Mastitis and
515 Udder Type Traits: A Random Regression Model for Joint Genetic Evaluation of Udder Health in
516 Denmark, Finland and Sweden. In: *Interbull Bulletin*. 2010. p. 25–32.
- 517 5. Jamrozik J, Koeck A, Miglior F, Kistemaker GJ, Schenkel FS, Kelton DF, et al. Genetic and Genomic
518 Evaluation of Mastitis Resistance in Canada. In: *Interbull Bulletin*. 2013. p. 43–51.
- 519 6. Pritchard T, Coffey M, Mrode R, Wall E. Genetic parameters for production, health, fertility and longevity
520 traits in dairy cows. *Animal.* 2013;7(1):34–46.
- 521 7. Sahana G, Guldbrandtsen B, Thomsen B, Holm LE, Panitz F, Brøndum RF, et al. Genome-wide
522 association study using high-density single nucleotide polymorphism arrays and whole-genome
523 sequences for clinical mastitis traits in dairy cattle. *J Dairy Sci* [Internet]. 2014;97(11):7258–75.
524 Available from: <http://dx.doi.org/10.3168/jds.2014-8141>
- 525 8. Abdel-Shafy H, Bortfeldt RH, Reissmann M, Brockmann GA. Short communication: Validation of somatic
526 cell score-associated loci identified in a genome-wide association study in German Holstein cattle. *J*
527 *Dairy Sci* [Internet]. 2014;97(4):2481–6. Available from: <http://dx.doi.org/10.3168/jds.2013-7149>
- 528 9. Sahana G, Guldbrandtsen B, Thomsen B, Lund MS. Confirmation and fine-mapping of clinical mastitis
529 and somatic cell score QTL in Nordic Holstein cattle. *Anim Genet.* 2013;44(6):620–6.
- 530 10. Sodeland M, Kent MP, Olsen HG, Opsal MA, Svendsen M, Sehested E, et al. Quantitative trait loci for
531 clinical mastitis on chromosomes 2, 6, 14 and 20 in Norwegian Red cattle. *Anim Genet.*
532 2011;42(5):457–65.
- 533 11. Veerkamp RF, Bouwman AC, Schrooten C, Calus MPL. Genomic prediction using preselected DNA
534 variants from a GWAS with whole-genome sequence data in Holstein-Friesian cattle. *Genet Sel Evol.*
535 2016;48(1):1–14.
- 536 12. Freebern E, Santos DJA, Fang L, Jiang J, Parker Gaddis KL, Liu GE, et al. GWAS and fine-mapping of
537 livability and six disease traits in Holstein cattle. *BMC Genomics.* 2020;21(1):1–11.
- 538 13. Olsen HG, Knutzen TM, Lewandowska-Sabat AM, Grove H, Nome T, Svendsen M, et al. Fine mapping of
539 a QTL on bovine chromosome 6 using imputed full sequence data suggests a key role for the group-
540 specific component (GC) gene in clinical mastitis and milk production. *Genet Sel Evol.* 2016;48(1):1–
541 16.
- 542 14. Cai Z, Guldbrandtsen B, Lund MS, Sahana G. Prioritizing candidate genes post-GWAS using multiple
543 sources of data for mastitis resistance in dairy cattle. *BMC Genomics.* 2018;19(1):1–11.
- 544 15. Tribout T, Croiseau P, Lefebvre R, Barbat A, Boussaha M, Fritz S, et al. Confirmed effects of candidate
545 variants for milk production, udder health, and udder morphology in dairy cattle. *Genet Sel Evol*
546 [Internet]. 2020;52(1):1–26. Available from: <https://doi.org/10.1186/s12711-020-00575-1>
- 547 16. Koivula M, Mäntysaari EA, Negussie E, Serenius T. Genetic and phenotypic relationships among milk
548 yield and somatic cell count before and after clinical mastitis. *J Dairy Sci.* 2005;88(2):827–33.
- 549 17. Cai Z, Dusza M, Guldbrandtsen B, Lund MS, Sahana G. Distinguishing pleiotropy from linked QTL
550 between milk production traits and mastitis resistance in Nordic Holstein cattle. *Genet Sel Evol*
551 [Internet]. 2020;52(1):19. Available from:
552 <https://gsejournal.biomedcentral.com/articles/10.1186/s12711-020-00538-6>
- 553 18. Jiang J, Ma L, Prakapenka D, VanRaden PM, Cole JB, Da Y. A large-scale genome-wide association study
554 in U.S. Holstein cattle. *Front Genet.* 2019;10(MAY).
- 555 19. Abo-Ismail MK, Brito LF, Miller SP, Sargolzaei M, Grossi DA, Moore SS, et al. Genome-wide association
556 studies and genomic prediction of breeding values for calving performance and body conformation traits
557 in Holstein cattle. *Genet Sel Evol.* 2017;49(82):1–29.
- 558 20. Nayeri S, Sargolzaei M, Abo-Ismail M, Miller S, Schenkel F, Moore S, et al. Genome-wide association
559 study for lactation persistency, female fertility, longevity, and lifetime profit index traits in Holstein
560 dairy cattle. *J Dairy Sci* [Internet]. 2017;100(2):1246–58. Available from:
561 <http://dx.doi.org/10.3168/jds.2016-11770>
- 562 21. Pausch H, Emmerling R, Schwarzenbacher H, Fries R. A multi-trait meta-analysis with imputed
563 sequence variants reveals twelve QTL for mammary gland morphology in Fleckvieh cattle. *Genet Sel*
564 *Evol.* 2016;48(1):1–9.
- 565 22. Xiang R, van den Berg I, MacLeod IM, Daetwyler HD, Goddard ME. Effect direction meta-analysis of
566 GWAS identifies extreme, prevalent and shared pleiotropy in a large mammal. *Commun Biol* [Internet].
567 2020;3(1):1–14. Available from: <http://dx.doi.org/10.1038/s42003-020-0823-6>
- 568 23. Gomme PT, Bertolini J. Therapeutic potential of vitamin D-binding protein. *TRENDS Biotechnol*
569 *Biotechnol.* 2004;22(7).
- 570 24. Horst RL, Reinhardt TA, Reddy GS. Vitamin D Metabolism. In: Feldman D, Pike JW, Adams JS, editors.
571 Vitamin D. 2nd ed. 2005. p. 15–36.

573 25. Jolliffe DA, Walton RT, Grif CJ, Martineau AR. Single nucleotide polymorphisms in the vitamin D
574 pathway associating with circulating concentrations of vitamin D metabolites and non-skeletal health
575 outcomes : Review of genetic association studies. *J Steroid Biochem Mol Biol.* 2016;164:18–29.

576 26. Poindexter MB, Kweh MF, Zimpel R, Zuniga J, Lopera C, Zenobi MG, et al. Feeding supplemental 25-
577 hydroxyvitamin D 3 increases serum mineral concentrations and alters mammary immunity of lactating
578 dairy cows. *J Dairy Sci.* 2020;103:805–22.

579 27. Merriman KE, Powell JL, Santos JEP, Nelson CD. Intramammary 25-hydroxyvitamin D3 treatment
580 modulates innate immune responses to endotoxin-induced mastitis. *J Dairy Sci [Internet].*
581 2018;101(8):7593–607. Available from: <http://dx.doi.org/10.3168/jds.2017-14143>

582 28. Zimin A V., Delcher AL, Florea L, Kelley DR, Schatz MC, Puiu D, et al. A whole-genome assembly of the
583 domestic cow, *Bos taurus*. *Genome Biol.* 2009;10(4).

584 29. CRV. Breeding value Udder Health (Manual Quality, Chapter E-27) [Internet]. 2020 [cited 2020 Aug
585 25]. Available from: https://cooperativecrv-be6.kxcdn.com/wp-content/uploads/2020/04/E_27-Uiergezondheid-April-2020-Engels.pdf

587 30. Gallagher MD, Chen-plotkin AS. The Post-GWAS Era : From Association to Function. *Am J Hum Genet*
588 [Internet]. 2018;102(5):717–30. Available from: <https://doi.org/10.1016/j.ajhg.2018.04.002>

589 31. Kommadath A, Grant JR, Krivushin K, Butty AM, Baes CF, Carthy TR, et al. A large interactive visual
590 database of copy number variants discovered in taurine cattle. *Gigascience.* 2019;8(6):1–12.

591 32. Gautier M, Klassmann A, Vitalis R. rehh 2.0: a reimplementation of the R package rehh to detect
592 positive selection from haplotype structure. *Mol Ecol Resour.* 2017;17(1):78–90.

593 33. Voight BF, Kudaravalli S, Wen X, Pritchard JK. A map of recent positive selection in the human genome.
594 *PLoS Biol [Internet].* 2006;4(3):e72. Available from: <http://www.ncbi.nlm.nih.gov/pubmed/16494531>

595 34. Miglior F, Fleming A, Malchiodi F, Brito LF, Martin P, Baes CF. A 100-Year Review: Identification and
596 genetic selection of economically important traits in dairy cattle. *J Dairy Sci [Internet].*
597 2017;100(12):10251–71. Available from: <http://dx.doi.org/10.3168/jds.2017-12968>

598 35. Ardlie KG, DeLuca DS, Segrè A V., Sullivan TJ, Young TR, Gelfand ET, et al. The Genotype-Tissue
599 Expression (GTEx) pilot analysis: Multitissue gene regulation in humans. *Science.*
600 2015;348(6235):648–60.

601 36. Brawand D, Soumilon M, Necsulea A, Julien P, Csárdi G, Harrigan P, et al. The evolution of gene
602 expression levels in mammalian organs. *Nature.* 2011;478(7369):343–8.

603 37. Lizio M, Abugessaïsa I, Noguchi S, Kondo A, Hasegawa A, Hon CC, et al. Update of the FANTOM web
604 resource: Expansion to provide additional transcriptome atlases. *Nucleic Acids Res.* 2019;47(D1):D752–
605 8.

606 38. Fagerberg L, Hallstrom BM, Oksvold P, Kampf C, Djureinovic D, Odeberg J, et al. Analysis of the human
607 tissue-specific expression by genome-wide integration of transcriptomics and antibody-based
608 proteomics. *Mol Cell Proteomics.* 2014;13(2):397–406.

609 39. Papatheodorou I, Fonseca NA, Keays M, Tang YA, Barrera E, Bazant W, et al. Expression Atlas: Gene
610 and protein expression across multiple studies and organisms. *Nucleic Acids Res.* 2018;46(D1):D246–
611 51.

612 40. The ENCODE Project Consortium. An integrated encyclopedia of DNA elements in the human genome.
613 *Nature.* 2012;489(7414):57–74.

614 41. Fang L, Sahana G, Su G, Yu Y, Zhang S. Integrating Sequence-based GWAS and RNA-Seq Provides
615 Novel Insights into the Genetic Basis of Mastitis and Milk Production in Dairy Cattle. *Sci Rep.*
616 2017;7(45560):1–16.

617 42. Zhu Z, Zhang F, Hu H, Bakshi A, Robinson MR, Powell JE, et al. Integration of summary data from
618 GWAS and eQTL studies predicts complex trait gene targets. *Nat Genet.* 2016;48(5).

619 43. Villar D, Berthelot C, Aldridge S, Rayner TF, Lukk M, Pignatelli M, et al. Enhancer evolution across 20
620 mammalian species. *Cell [Internet].* 2015;160(3):554–66. Available from:
621 <http://dx.doi.org/10.1016/j.cell.2015.01.006>

622 44. Cao Y, Chen G, Wu G, Zhang X, McDermott J, Chen X, et al. Widespread roles of enhancer-like
623 transposable elements in cell identity and long-range genomic interactions. *Genome Res.*
624 2019;29(1):40–52.

625 45. Heinz S, Benner C, Spann N, Bertolino E, Lin YC, Laslo P, et al. Simple Combinations of Lineage-
626 Determining Transcription Factors Prime cis-Regulatory Elements Required for Macrophage and B Cell
627 Identities. *Mol Cell [Internet].* 2010;38(4):576–89. Available from:
628 <http://dx.doi.org/10.1016/j.molcel.2010.05.004>

629 46. Sudmant PH, Rausch T, Gardner EJ, Handsaker RE, Abyzov A, Huddleston J, et al. An integrated map of
630 structural variation in 2,504 human genomes. *Nature.* 2015;526(7571):75–81.

631 47. Handsaker RE, Van Doren V, Berman JR, Genovese G, Kashin S, Boettger LM, et al. Large multiallelic
632 copy number variations in humans. *Nat Genet [Internet].* 2015;47(3):296–303. Available from:
633 <http://dx.doi.org/10.1038/ng.3200>

634 48. Hekselman I, Yeger-Lotem E. Mechanisms of tissue and cell-type specificity in heritable traits
635 and diseases. *Nat Rev Genet [Internet].* 2020; Available from:
636 <http://www.ncbi.nlm.nih.gov/pubmed/31913361>

637 49. Littlejohn MD, Tiplady K, Lopdell T, Law TA, Scott A, Harland C, et al. Expression variants of the
638 lipogenic AGPAT6 gene affect diverse milk composition phenotypes in *Bos taurus*. *PLoS One.*
639 2014;9(1):1–12.

640 50. Littlejohn MD, Tiplady K, Fink TA, Lehnert K, Lopdell T, Johnson T, et al. Sequence-based Association
641 Analysis Reveals an MGST1 eQTL with Pleiotropic Effects on Bovine Milk Composition. *Sci Rep.*
642 2016;(May):1–14.

643 51. Kemper KE, Littlejohn MD, Lopdell T, Hayes BJ, Bennett LE, Williams RP, et al. Leveraging genetically
644 simple traits to identify small-effect variants for complex phenotypes. *BMC Genomics*. 2016;17(1):1–9.
645 52. Brand B, Scheinhardt MO, Friedrich J, Zimmer D, Reinsch N, Ponsuksili S, et al. Adrenal cortex
646 expression quantitative trait loci in a German Holstein × Charolais cross. *BMC Genet*. 2016;17(1):1–11.
647 53. Lopdell TJ, Tiplady K, Struchalin M, Johnson TJ, Keehan M, Sherlock R, et al. DNA and RNA-sequence
648 based GWAS highlights membrane-transport genes as key modulators of milk lactose content. *BMC
649 Genomics*. 2017;18(1):1–18.
650 54. Leal-Gutiérrez JD, Elzo MA, Mateescu RG. Identification of eQTLs and sQTLs associated with meat
651 quality in beef. *BMC Genomics*. 2020;21(1):1–15.
652 55. Van Den Berg I, Hayes BJ, Chamberlain AJ, Goddard ME. Overlap between eQTL and QTL associated
653 with production traits and fertility in dairy cattle. *BMC Genomics*. 2019;20(1):1–18.
654 56. Ngcungcu T, Oti M, Sitek JC, Haukanes BI, Linghu B, Brucolari R, et al. Duplicated Enhancer Region
655 Increases Expression of CTSB and Segregates with Keratolytic Winter Erythema in South African and
656 Norwegian Families. *Am J Hum Genet* [Internet]. 2017;100(5):737–50. Available from:
657 <http://dx.doi.org/10.1016/j.ajhg.2017.03.012>
658 57. Long HK, Prescott SL, Wysocka J. Ever-Changing Landscapes: Transcriptional Enhancers in
659 Development and Evolution. *Cell* [Internet]. 2016;167(5):1170–87. Available from:
660 <http://dx.doi.org/10.1016/j.cell.2016.09.018>
661 58. Scholes C, Biette KM, Harden TT, DePace AH. Signal Integration by Shadow Enhancers and Enhancer
662 Duplications Varies across the *Drosophila* Embryo. *Cell Rep* [Internet]. 2019;26(9):2407–2418.e5.
663 Available from: <https://doi.org/10.1016/j.celrep.2019.01.115>
664 59. Osterwalder M, Barozzi I, Tissières V, Fukuda-yuzawa Y, Mannion BJ, Afzal SY, et al. Enhancer
665 redundancy provides phenotypic robustness in mammalian development. *Nat Publ Gr*. 2018;
666 60. Giuffra E, Tuggle CK. Functional Annotation of Animal Genomes (FAANG): Current Achievements and
667 Roadmap. *Annu Rev Anim Biosci*. 2019;7:65–88.
668 61. The FAANG Consortium, Andersson L, Archibald AL, Bottema CD, Brauning R, Burgess SC, et al.
669 Coordinated international action to accelerate genome-to-phenome with FAANG, the Functional
670 Annotation of Animal Genomes project. *Genome Biol*. 2015;16(1):4–9.
671 62. Hedrick PW. Heterozygote Advantage : The Effect of Artificial Selection in Livestock and Pets. *J Hered*.
672 2015;106(2):141–54.
673 63. Georges M, Charlier C, Hayes B. Harnessing genomic information for livestock improvement. *Nat Rev
674 Genet* [Internet]. 2019;20(3):135–56. Available from: <http://dx.doi.org/10.1038/s41576-018-0082-2>
675 64. Georges M. Mapping , Fine Mapping , and Molecular Dissection of Quantitative Trait Loci in Domestic
676 Animals. *Annu Rev Genomics Hum Genet*. 2007;8:131–62.
677 65. Daiger SP, Mel S, Cavalli-Sforza LL. Group-Specific Component (Gc) Proteins Bind Vitamin D and 25-
678 Hydroxyvitamin D. *Proc Nati Acad Sci*. 1975;72(6):2076–80.
679 66. Bouillon R, Schuit F, Antonio L, Rastinejad F. Vitamin D Binding Protein: A Historic Overview. *Front
680 Endocrinol (Lausanne)*. 2020;10(January):1–21.
681 67. Yamamoto N, Kumashiro R. Conversion of vitamin D3 binding protein (group-specific component) to a
682 macrophage activaating factor by the stepwise action of beta-galactosidase of B cells and sialidase of T
683 cells. *J Immunol*. 1993;151:2794–802.
684 68. Swamy N, Dutta A, Ray R. Roles of the structure and orientation of ligands and ligand mimics inside the
685 ligand-binding pocket of the vitamin D-binding protein. *Biochemistry*. 1997;36(24):7432–6.
686 69. Bikle DD, Schwartz J. Vitamin D binding protein, total and free Vitamin D levels in different
687 physiological and pathophysiological conditions. *Front Endocrinol (Lausanne)*. 2019;10(MAY):1–12.
688 70. Chun RF, Peercy BE, Orwoll ES, Nielson CM, Adams JS, Hewison M. Vitamin D and DBP: The free
689 hormone hypothesis revisited. *J Steroid Biochem Mol Biol* [Internet]. 2014;144(PART A):132–7.
690 Available from: <http://dx.doi.org/10.1016/j.jsbmb.2013.09.012>
691 71. Sinotte M, Diorio C, Berube S, Pollak M, Brisson J. Genetic polymorphisms of the vitamin D binding
692 protein and plasma concentrations of 25-hydroxyvitamin D in premenopausal women. *Am J Clin Nutr*.
693 2009;25(3):634–40.
694 72. Lauridsen AL, Vestergaard P, Hermann AP, Brot C, Heickendorff L, Mosekilde L, et al. Plasma
695 concentrations of 25-Hydroxy-Vitamin D and 1,25-Dihydroxy-Vitamin D are Related to the Phenotype of
696 Gc (Vitamin D-Binding Protein): A Cross-sectional Study on 595 Early Postmenopausal Women. *Calcif
697 Tissue Int*. 2005;25:15–22.
698 73. Autier P, Boniol M, Pizot C, Mullie P. Vitamin D status and ill health : a systematic review. *Lancet
699 Diabetes Endocrinol*. 2014;2(January):76–89.
700 74. Santos JEP, Bisinotto RS, Ribeiro ES. Mechanisms underlying reduced fertility in anovular dairy cows.
701 *Theriogenology* [Internet]. 2016;86(1):254–62. Available from:
702 <http://dx.doi.org/10.1016/j.theriogenology.2016.04.038>
703 75. Irani M, Merhi Z, D M. Role of vitamin D in ovarian physiology and its implication in reproduction : a
704 systematic review. *Fertil Steril* [Internet]. 2014;102(2):460–468.e3. Available from:
705 <http://dx.doi.org/10.1016/j.fertnstert.2014.04.046>
706 76. Dechow CD, Rogers GW, Sander-Nielsen U, Klei L, Lawlor TJ, Clay JS, et al. Correlations among body
707 condition scores from various sources, dairy farm, and cow health from the United States and Denmark.
708 *J Dairy Sci* [Internet]. 2004;87(10):3526–33. Available from: [http://dx.doi.org/10.3168/jds.S0022-0302\(04\)73489-X](http://dx.doi.org/10.3168/jds.S0022-
709 0302(04)73489-X)
710 77. Li H. Aligning sequence reads, clone sequences and assembly contigs with BWA-MEM. *arXiv Prepr arXiv*
711 [Internet]. 2013;00(00):3. Available from: <http://arxiv.org/abs/1303.3997>
712 78. Li H, Durbin R. Fast and accurate short read alignment with Burrows-Wheeler transform. *Bioinformatics*.
713 2009;25(14):1754–60.

714 79. Tarasov A, Vilella AJ, Cuppen E, Nijman IJ, Prins P. Sambamba : fast processing of NGS alignment
715 formats. *Bioinfo*. 2015;31(February):2032–4.

716 80. Kadri NK, Harland C, Faux P, Cambisano N, Karim L, Coppelters W, et al. Coding and noncoding
717 variants in HFM1, MLH3, MSH4, MSH5, RNF212, and RNF212B affect recombination rate in cattle.
718 *Genome Res*. 2016;1323–32.

719 81. Kadri N, Charlier C, Cambisano N, Deckers M, Mullaart E. High resolution mapping of cross-over events
720 in cattle using NGS data. In: *Proceedings of the World Congress on Genetics Applied to Livestock
721 Production*. 2018. p. 11.808.

722 82. Browning BL, Zhou Y, Browning SR. A One-Penny Imputed Genome from Next-Generation Reference
723 Panels. *Am J Hum Genet* [Internet]. 2018;103(3):338–48. Available from:
724 <https://doi.org/10.1016/j.ajhg.2018.07.015>

725 83. Yang J, Lee SH, Goddard ME, Visscher PM. GCTA: A tool for genome-wide complex trait analysis. *Am J
726 Hum Genet* [Internet]. 2011;88(1):76–82. Available from:
727 <http://dx.doi.org/10.1016/j.ajhg.2010.11.011>

728 84. Yang J, Zaitlen NA, Goddard ME, Visscher PM, Price AL. Advantages and pitfalls in the application of
729 mixed-model association methods. *Nat Genet*. 2014;46(2).

730 85. Faust GG, Hall IM. SAMBLASTER : fast duplicate marking and structural variant read extraction.
731 *Bioinformatics*. 2014;30(17):2503–5.

732 86. Layer RM, Chiang C, Quinlan AR, Hall IM. LUMPY : a probabilistic framework for structural variant
733 discovery. *Genome Biol*. 2014;15(R84):1–19.

734 87. Pedersen BS, Quinlan AR. Duphold : scalable , depth-based annotation and curation of high-confidence
735 structural variant calls. *Gigascience*. 2019;(March):1–5.

736 88. Druet T, Georges M. LINKPHASE3: An improved pedigree-based phasing algorithm robust to genotyping
737 and map errors. *Bioinformatics*. 2015;31(10):1677–9.

738 89. Bertrand AR, Flori L, Druet T. RZooRoH : An R package to characterize individual genomic autozygosity
739 and identify homozygous-by-descent segments. *Methods Ecol Evol*. 2019;2019(10):860–6.

740 90. Druet T, Gautier M. A model-based approach to characterize individual inbreeding at both global and
741 local genomic scales. *Mol Ecol*. 2017;26:5820–41.

742 91. Boichard D, Boussaha M, Capitan A, Rocha D, Sanchez MP, Tribout T, et al. Experience from large scale
743 use of the EuroGenomics custom SNP chip in cattle. In: *11th World Congress on Genetics Applied to
744 Livestock Production*. 2018. p. 1–6.

745 92. Liu B, Gloudemann MJ, Rao AS, Ingelsson E, Montgomery SB. Abundant associations with gene
746 expression complicate GWAS follow-up. *Nat Genet* [Internet]. 2019;51(May). Available from:
747 <http://dx.doi.org/10.1038/s41588-019-0404-0>

748 93. Kim D, Paggi JM, Park C, Bennett C, Salzberg SL. Graph-based genome alignment and genotyping with
749 HISAT2 and HISAT-genotype. *Nat Biotechnol* [Internet]. 2019;37(August). Available from:
750 <http://dx.doi.org/10.1038/s41587-019-0201-4>

751 94. Pertea M, Pertea GM, Antonescu CM, Chang T-C, Mendell JT, Salzberg SL. StringTie enables improved
752 reconstruction of a transcriptome from RNA-seq reads. *Nat Biotech*. 2016;33(3):290–5.

753 95. Love MI, Huber W, Anders S. Moderated estimation of fold change and dispersion for RNA-seq data with
754 DESeq2. *Genome Biol*. 2014;15(12):1–21.

755 96. Stegle O, Parts L, Piipari M, Winn J, Durbin R. Using probabilistic estimation of expression residuals
756 (PEER) to obtain increased power and interpretability of gene expression analyses. 2012;7(3):500–7.

757 97. Shabalin AA. Matrix eQTL : ultra fast eQTL analysis via large matrix operations. *Bioinformatics*.
758 2012;28(10):1353–8.

759 98. Hunt SE, McLaren W, Gil L, Thormann A, Schuilenburg H, Sheppard D, et al. Ensembl variation
760 resources. 2018;(8):1–12.

761 99. Zhang Y, Liu T, Meyer CA, Eeckhoute J, Johnson DS, Bernstein BE, et al. Model-based Analysis of ChIP-
762 Seq (MACS). *Genome Biol*. 2008;(9):R137.

763 100. Kent WJ, Sugnet CW, Furey TS, Roskin KM, Pringle TH, Zahler AM, et al. The Human Genome Browser
764 at UCSC. *Genome Res*. 2002;12(6):996–1006.

765 101. de Souza MM, Zerlotini A, Geistlinger L, Tizioto PC, Taylor JF, Rocha MIP, et al. A comprehensive
766 manually-curated compendium of bovine transcription factors. *Sci Rep* [Internet]. 2018;8(1):1–12.
767 Available from: <http://dx.doi.org/10.1038/s41598-018-32146-2>

768 102. Liu X, Yu X, Zack DJ, Zhu H, Qian J. TiGER: A database for tissue-specific gene expression and
769 regulation. *BMC Bioinformatics*. 2008;9:1–7.

770 103. Barrett JC, Fry B, Maller J, Daly MJ. Haploview: Analysis and visualization of LD and haplotype maps.
771 *Bioinformatics*. 2005;21(2):263–5.

772

774 **Figures**

775

776 **Figure 1. Association mapping of clinical mastitis resistance on BTA6**

777 (A) Association mapping performed with imputed BovineHD variants on BTA6. The association signal near BTA 6:88.6 Mb, shown in
778 other dairy cattle populations was replicated in the current Dutch HF population. (B) Association mapping performed with imputed
779 WGS variants in BTA 6:84-93 Mb region. A strong association signal was shown in a 200 Kb region (BTA 6:88.5-88.7 Mb), spanning
780 over *GC* gene. Our lead SNP (rs110813063, marked with green and vertical dotted line) has not been reported as a candidate SNP in
781 other CM fine-mapping studies. CM candidate SNPs from other fine-mapping studies are marked as yellow. (C) Conditional analyses
782 including GC CNV as a covariate nullify the association signal.

783

784 **Figure 2. Discovery of multiallelic GC duplication using deeply sequenced genomes and familial structure**

785 (A) Schematic overview showing the GWAS lead SNP and ~12 kb CNV overlapping with *GC*. *GC* is a reverse oriented gene, consisting
786 of 14 exons, of which two last exons are non-coding. Five CNV tagging SNPs were present within the GC CNV and marked with black
787 asterisks (the middle asterisk covers three tagging SNPs). Among them, the first SNP, which was also the GWAS lead SNP, was in
788 perfect LD with the GC CNV ($r^2 = 1$), whereas the rest were in high LD ($r^2 > 0.98$). The hash marks at the upstream and the intronic
789 region of *GC* indicate CM resistance candidate SNPs reported by others [13,14]. (B) Sequencing depth difference between the CNV
790 region and normal region was used to infer copy numbers. (C) A Histogram of read depth values shows that majority of animals fall
791 into diploid copy number of 2, 5 and 8, and some minor peaks occur at diploid copy number of 6, 7, 9 and 10. Based on this diploid
792 CNs, we inferred haploid CNs of 1, 4, 5, and 6. We showed possible allelic combination(s) above each diploid CN. The diploid CN10
793 could be comprised of CN5/CN5 and CN4/CN6, however, our results showed that it was always CN4/CN6. (D) Familial information
794 and background haplotypes were used to phase the copy number and thus revealed how the CNV segregates in trios. The upper
795 family tree shown with animal signs stands for diploid copy numbers, whereas the lower tree shows haploid copy numbers (the
796 phase results of the diploid CNs).

797

798 **Figure 3. Characterization of the GC CNV tagging SNPs and allelic imbalance pattern**

799 (A) A schematic overview of four structural haplotypes and the five tagging SNPs inside the GC CNV, shown together with allele
800 frequencies. (B) Positions, rs ID, alleles, location within GC of GC CNV tagging SNPs. (C) Allelic imbalance pattern shown in Wt/Dup
801 animals. Animals will get more supporting reads for alternative alleles for the five CNV tagging SNPs, thus the tagging SNPs will be
802 called as heterozygous but with high allelic imbalance

803

804 **Figure 4. Selection signature scan and trait association (clinical mastitis resistance and milk yield) GWAS plot**

805 (A) A 10-Mb region with a strong selective signature signal was zoomed in (BTA 6: 84-93 Mb). Association mapping results from
806 imputed WGS variants on CM resistance (dark blue) and MY (yellow) are shown in the upper panel; iHS results are shown in the
807 lower panel. The CM resistance GWAS peak occurs at the left side of the iHS peak, whereas MY GWAS peak appears on the right side
808 of the iHS peak. The red vertical line marks GC CNV. A 1-Mb region covering GC CNV, iHS lead SNP, and MY lead SNP are marked with
809 translucent blue. (B) The extended haplotype homozygosity of the 1-Mb region marked in panel (A) is shown, together with four
810 genes annotated in this region (top of the figure). The major haplotype shown in the upper part (black) branches outwards, implying
811 recent positive selection acted upon this haplotype. The non-selected haplotype, shown in the lower side (blue) rapidly breaks down
812 from the iHS lead SNP. (C) Pairwise D' and r^2 values between GC CNV, iHS lead SNP, and MY lead SNP in the ~4,000 daughter proven
813 bulls. A screenshot made from Haplovview software [103].

814

815 **Figure 5. eQTL mapping and GWAS-eQTL colocalization results for GC and the non-coding RNA**

816 (A) A Schematic overview of the *GC* gene structure and position of the GC CNV. Our data detected two *GC* transcripts, where the
817 canonical form account the majority of the expression (98%) and an alternative form only counting for minor expression (2%). (B)
818 eQTL was mapped for the genes located in a 2-Mb bin (BTA6:87.68-89.68). Of the 13 genes annotated in this bin, *GC* showed
819 predominantly high expression (5,000 TPM <), whereas the rest were lowly expressed or not expressed at all. The eQTL were mapped
820 for *GC* and *SLC4A4*. (C) CM resistance GWAS results were shown for the 2-Mb bin, where eQTL was mapped. The color scale indicates
821 the degree of pair-wise LD (r^2) between the GC CNV and other SNPs. Annotation of genes in this region is drawn as black bars. Six
822 genes on the left part are *AMBN*, *JCHAIN*, *RUFY3*, *GRSF1*, *MOB1B*, and *DCK*. (D) eQTL mapping results for *GC* (canonical transcript).
823 (E) P-values obtained from CM resistance GWAS and *GC* (canonical transcript) eQTL mapping were correlated. The GC CNV is located
824 in the right upper corner ($p=0.68$), showing that it is significant for both GWAS and eQTL mapping. (F) The box plot shows altered *GC*
825 (canonical transcript) expression depending on GC CNV genotypes. (G) eQTL mapping result for *GC* (alternative transcript). (H) P-
826 values obtained from CM resistance GWAS and *GC* (alternative transcript) eQTL mapping were correlated. The GC CNV is located in
827 the right upper corner ($p=0.74$), showing that it is significant for both GWAS and eQTL mapping. (I) The box plot shows altered *GC*
828 (alternative transcript) expression depending on GC CNV genotypes. Panels C-E, G, H were made with LocusCompare programme
829 [92]

830

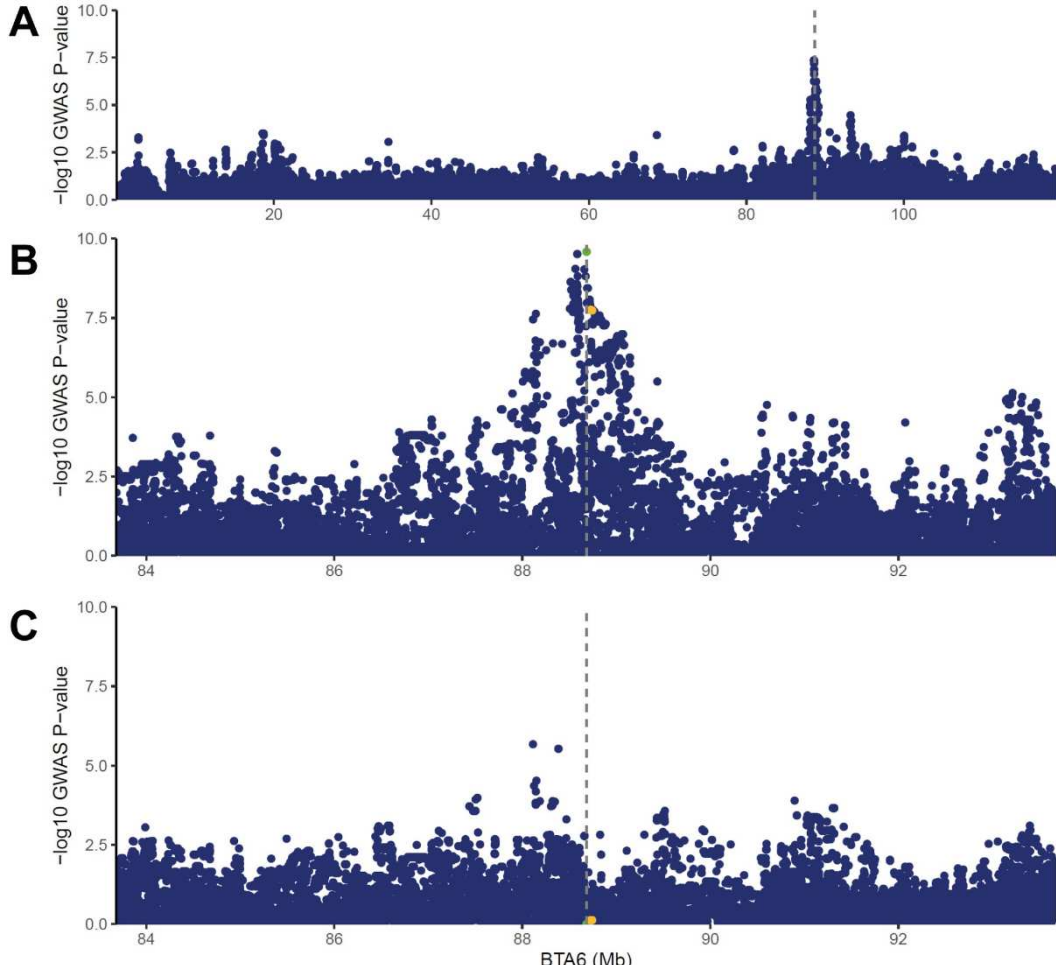
831 **Figure 6. Inspection of functional elements near the GC CNV**

832 Functional elements were inspected in *GC* eQTL region using ChIP-seq (H3K27ac and H3K4me3) and ATAC-seq data. (A) The *GC* eQTL
833 region was zoomed in. In this region, *GC* is the only annotated gene. The GC CNV is marked with the translucent blue, and CM
834 resistance candidate SNPs reported by other studies [13,14] are marked with translucent yellow. Other significant eQTL lead SNPs in
835 this region are marked with translucent pink. We overlaid ChIP-seq data to identify putative enhancers and promoters (ChIP-seq
836 tracks; red). Furthermore, liver ATAC-seq data revealed highly accessible chromatin regions, supporting the regulatory elements
837 discovered by ChIP-seq data sets (ATAC-seq tracks; blue). (B) We further zoomed in to the ATAC peak within the GC CNV, and

838 discovered that the ATAC peak overlaps with MER 115. The predicted hepatic transcription factor binding sites are marked with
 839 translucent grey. (C) Transcription factor binding motifs are shown together with the ATAC signal located inside the GC CNV.
 840

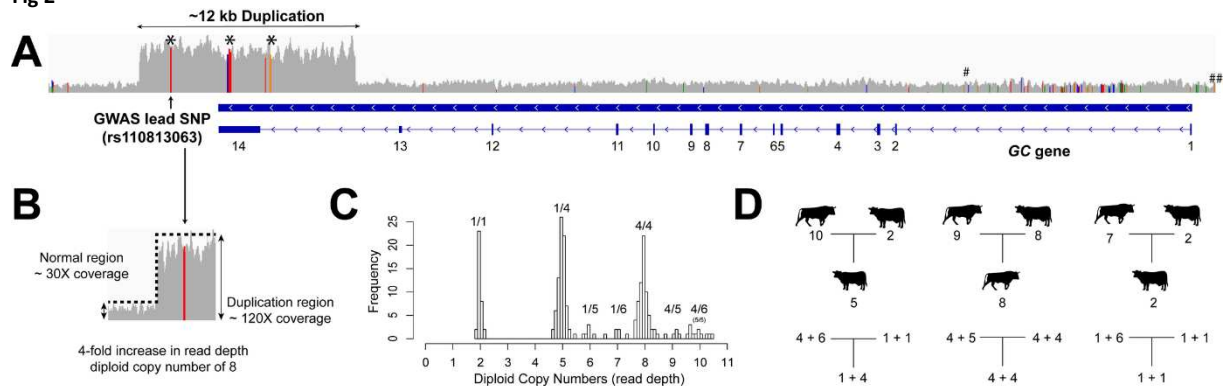
841 **Figure 7. Summary of the key findings and hypothesis of physiological aspects linking GC expression and CM resistance**
 842 A schematic overview summarizing the allele effects of wildtype (CN 1) and multiplicated (CNs 4-6) alleles of the GC CNV, a likely
 843 causal variant for the major CM resistance QTL. The two alleles at the GC CNV locus lead to altered GC transcription, where the
 844 multiplicated alleles correspond to high GC expression. On the bottom shows the phenotypic association between the GC CNV and
 845 CM resistance, where the multiplicated allele is associated with low CM resistance. Finally, the area marked with grey shade shows
 846 our hypotheses that the amount of DBP is positively related with the GC expression. Further, we speculated that the amount of DBP
 847 and free vitamin D is inversely correlated, as long as vitamin D is bound by DBP, it is not biologically available. The solid arrows
 848 indicate the relations based on our findings. The dotted arrows indicate the relations based on our speculation.
 849

850 **Fig 1**



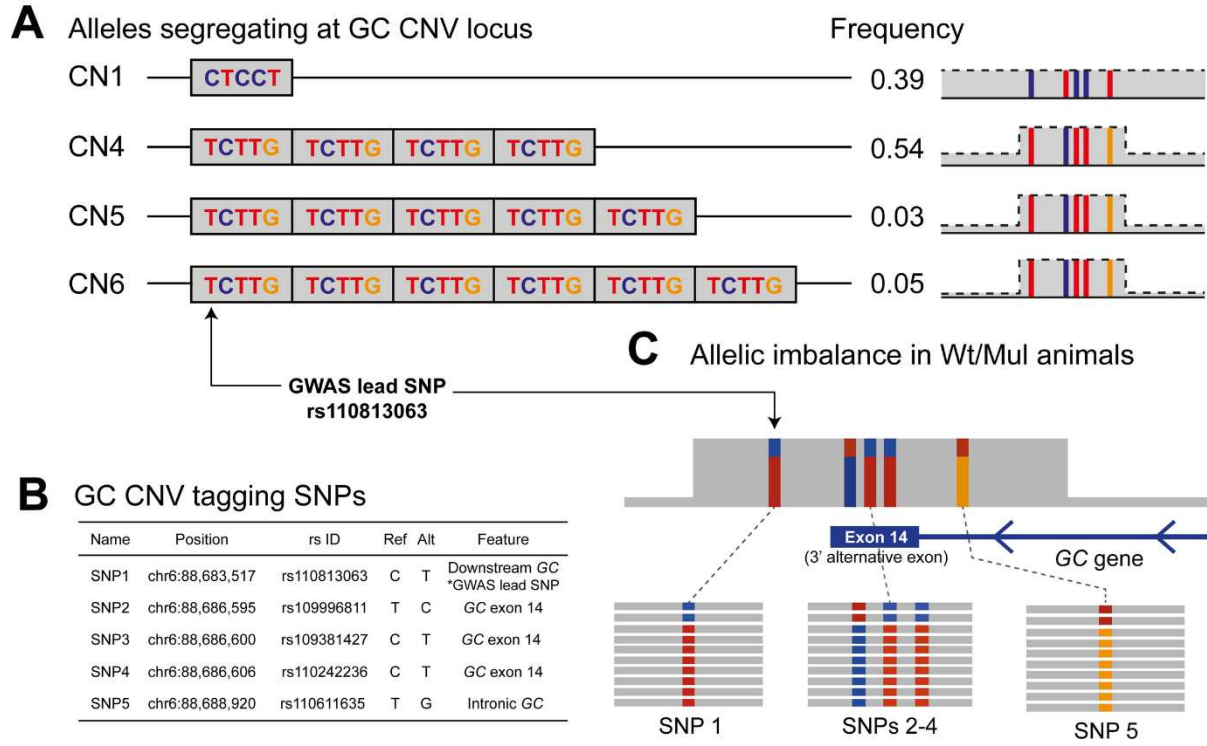
851
 852
 853

Fig 2



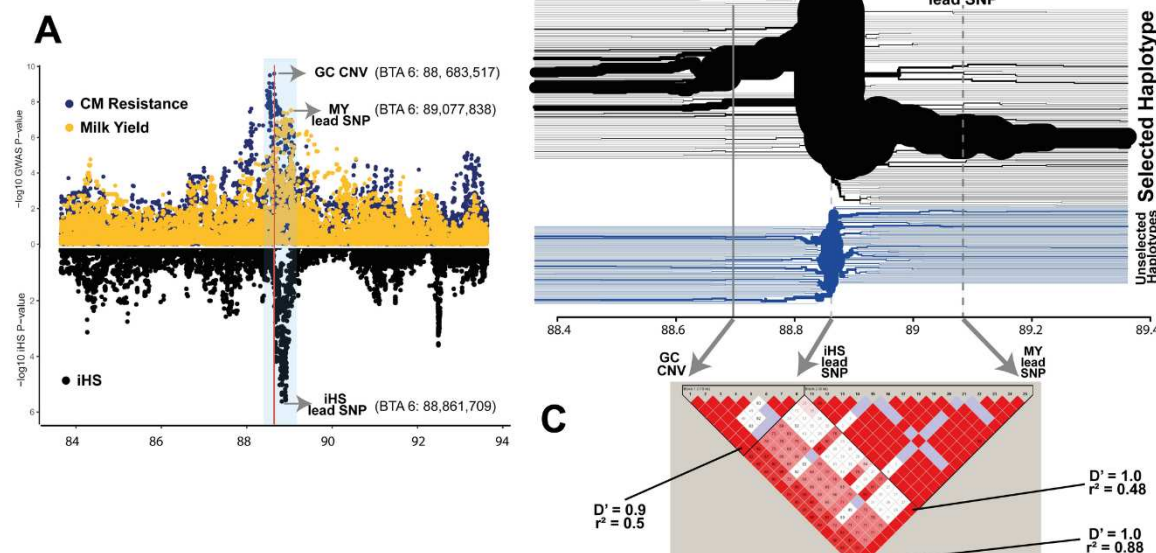
854
 855
 856

Fig 3



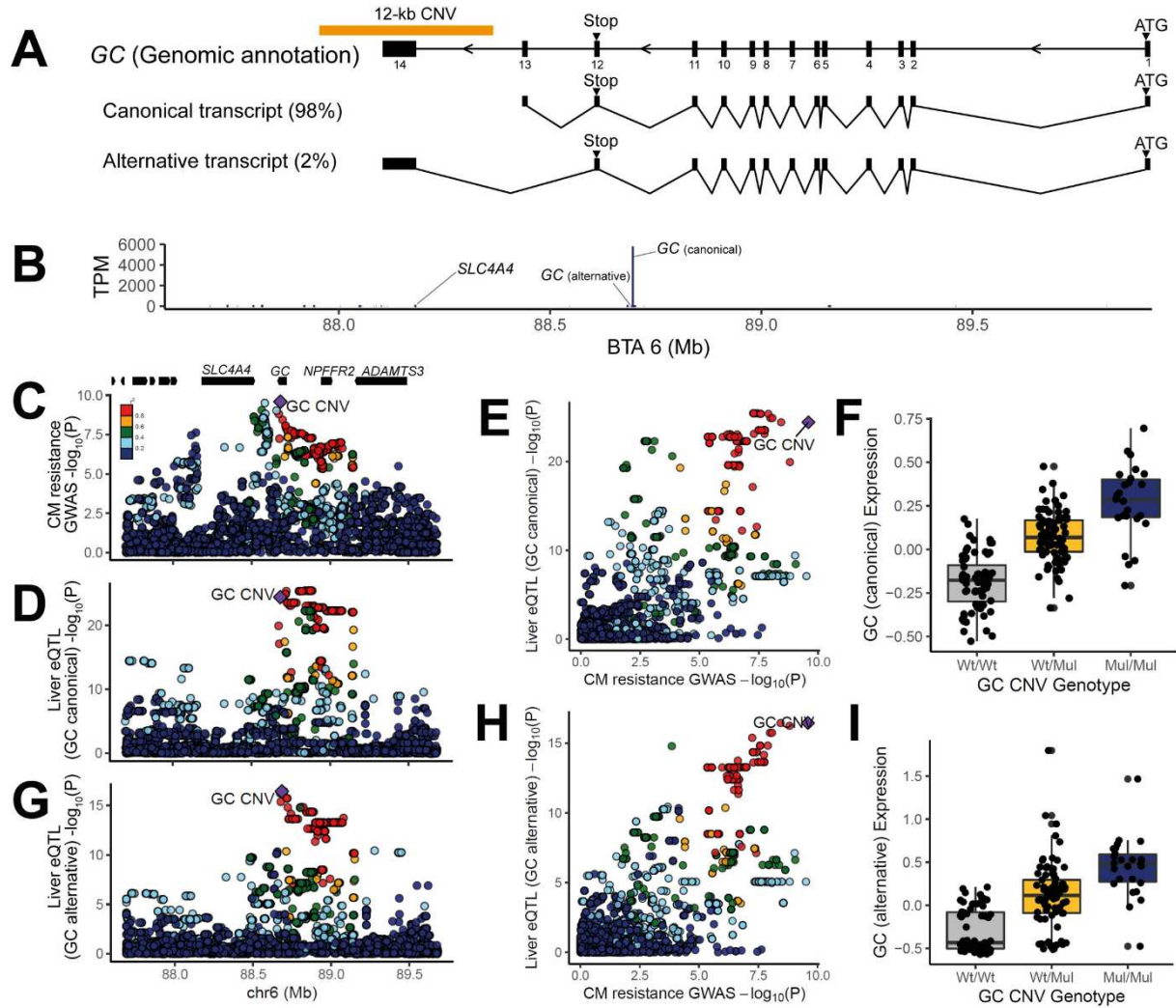
857
858
859

Fig 4



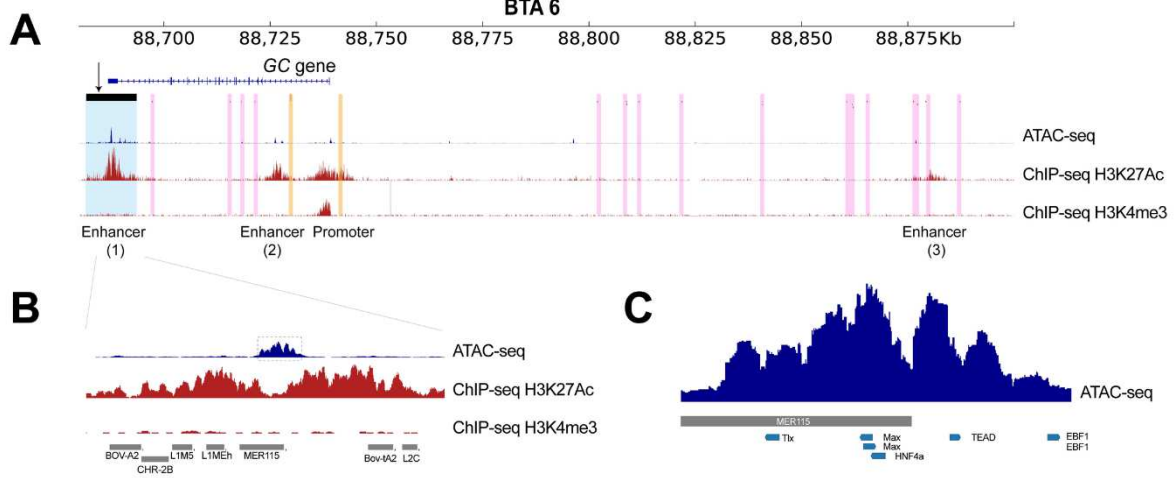
860
861
862

Fig 5



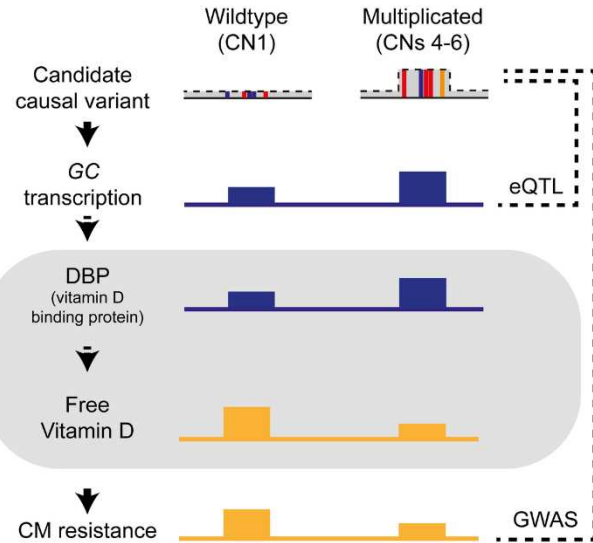
863
 864
 865

Fig 6



866
 867
 868

Fig 7



869
870

871 **Supporting information**

872

873

874 **S1 Figure. Manhattan plot for CM resistance GWAS results**

875 Genome-wide association mapping of the CM resistance trait, performed using imputed BovineHD data

876

877 **S2 Figure. IGV screen shots for the GC CNV and its' breakpoints**

878 (A) The GC CNV (BTA 6:88,681,767-88,693,553) is shown in the IGV screen shot. The grey reads are normally mapped reads, whereas
879 green ones are discordantly mapped reads, providing evidence for a tandem duplication. The sequencing coverage of the CNV region
880 is higher than non-CNV region. (B) The left breakpoint is flanked by MIR repeat. (C) The right breakpoint does not overlap with repeats.
881 (D and E) The left and right breakpoints are zoomed in and the soft-clipped reads (positions where nucleotide sequences are written)
882 information revealed the 5-bp microhomology "CACAT" (marked as yellow) at the breakpoints.

883

884 **S3 Figure. Family tree of animals having CN 5 and CN6 allele on GC CNV locus**

885 In the panel of 266 animals, we observed CN 5 and CN6 alleles are mostly segregating among a small number of related animals. To
886 show that CN5 and CN6 alleles are truly segregating, transmission probabilities at each marker position were calculated with
887 LINKPHASE3. Transmission probabilities were estimated for paternal haplotypes (1 and 0 indicated transmission of the paternal and
888 maternal allele, respectively). (A) Largest family of CN5 carriers. Each circle indicates one individual and the number inside the circle
889 indicates the GC CNV copy number genotype. The numbers above each individual stand for the transmission probability. Questions
890 marks mean individuals with no copy number information. Male animals are shown as squares, female animals are shown as circles,
891 and animals with unknown gender are marked with diamonds. (B) Largest family of CN6 carriers. The legends are identical to panel
892 (A).

893

894 **S4 Figure. Chromosome-wide scan of selection signatures using integrated Haplotype Score (iHS) on BTA6**

895 Chromosome-wide scan of integrated Haplotype Score revealed two iHS peaks with high significance ($-\log_{10}P > 5$), near BTA6:78
896 Mb and BTA6:89 Mb.

897

898 **S5 Figure. Three traits that showed strong association signals in CM resistance QTL region on BTA 6**

899 Colocalization of fine-mapping p-values of a pair of traits are showing that body condition score (BCS), calving interval (CI), and milk
900 yield (MY) are having association signal near or at the CM resistance QTL region on BTA 6. (A) Colocalization between body condition
901 score and CM resistance is shown in the left panel, together with the separate Manhattan plots for body condition score and CM
902 resistance on the right. (B) Colocalization between calving interval and CM resistance. (C) Colocalization between milk yield and CM
903 resistance. Panel layout of (B) and (C) is the same as panel (A). In each panel, the colours of dots indicate degree of LD (r^2) with GC
904 CNV (colour scale shown in the left upper corner of panel A). The purple diamond marks GC CNV. The figure was made with
905 LocusCompare programme [92].

906

907

908 **S6 Figure. eQTL mapping and GWAS-eQTL colocalization results for SLC4A4**

909 A colocalization plot for CM resistance GWAS and *SLC4A4* eQTL mapping results is shown on the left side. The right upper panel is
910 the CM resistance GWAS results and the right lower panel is the *SLC4A4* eQTL mapping results. In between these two right panels
911 are the genes located in this region. Six genes on the left part are *AMBN*, *JCHAIN*, *RUFY3*, *GRSF1*, *MOB1B*, and *DCK*. In each panel,
912 the colours of dots indicate degree of LD (r^2) with GC CNV (colour scale shown in the left upper corner of the colocalization figure).
913 The purple diamond marks GC CNV.

914

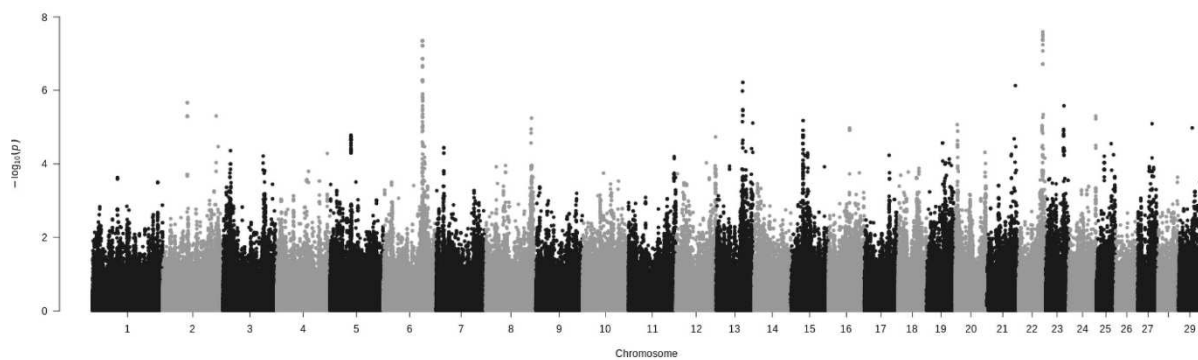
915

916

917

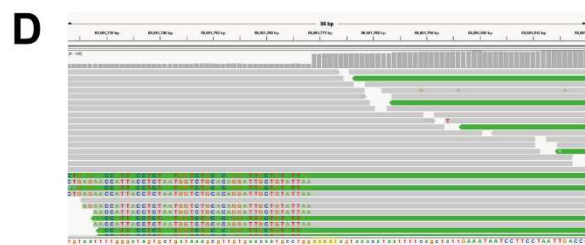
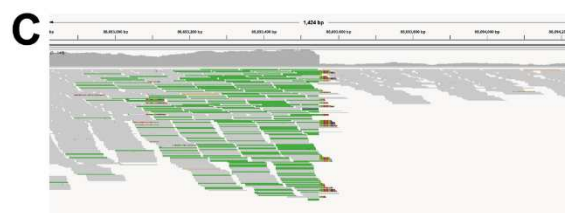
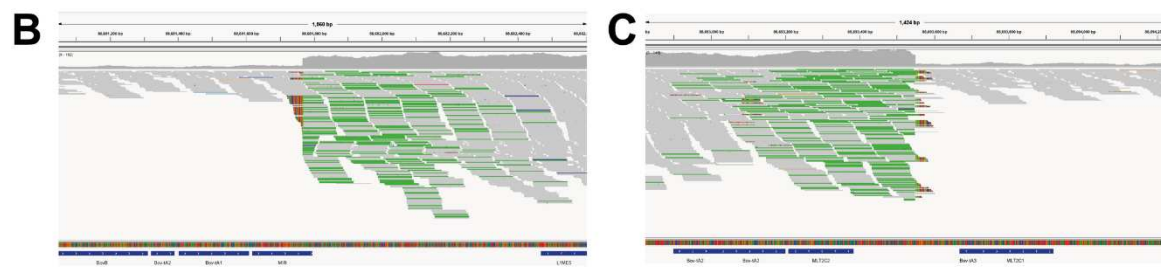
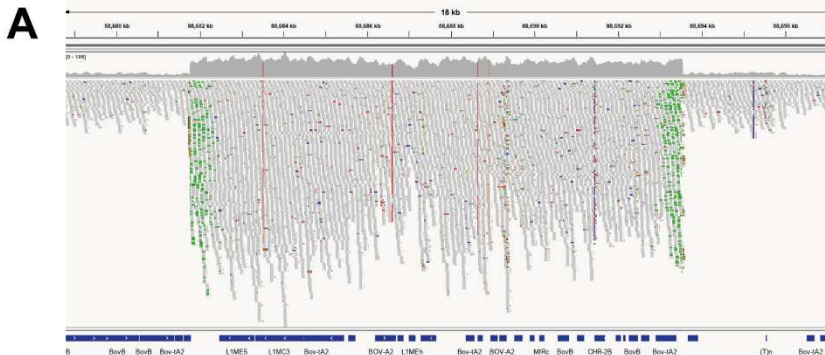
918

919 **S1 Fig**



920
921
922

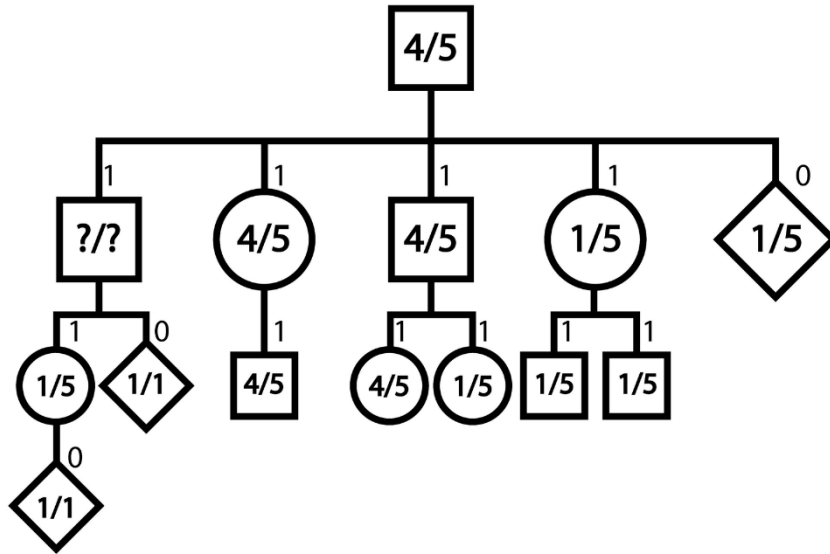
S2 Fig



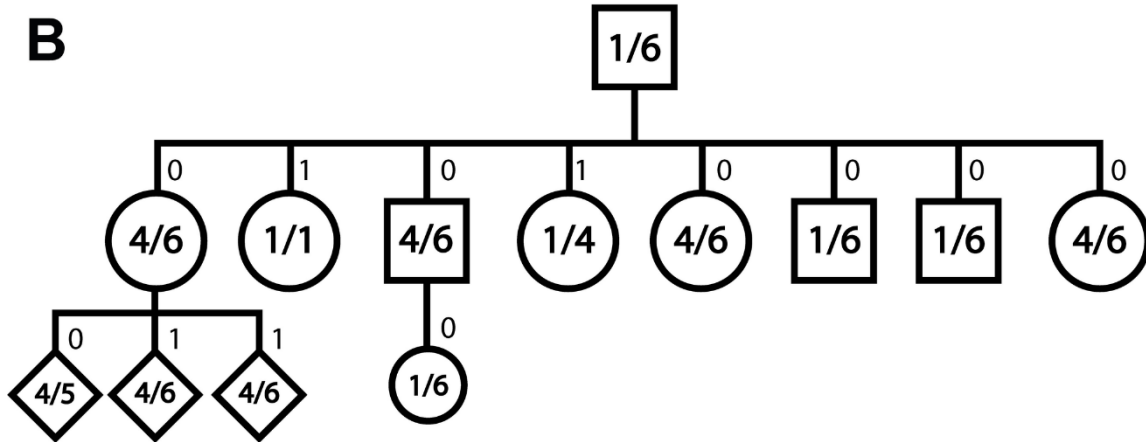
923
924
925

S3 Fig

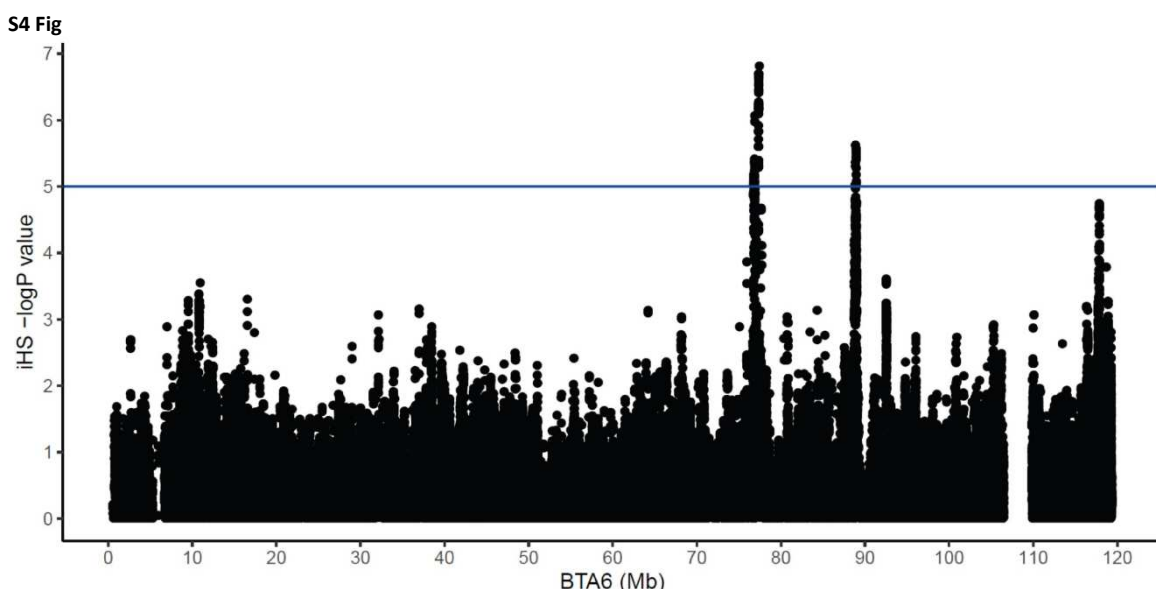
A



B

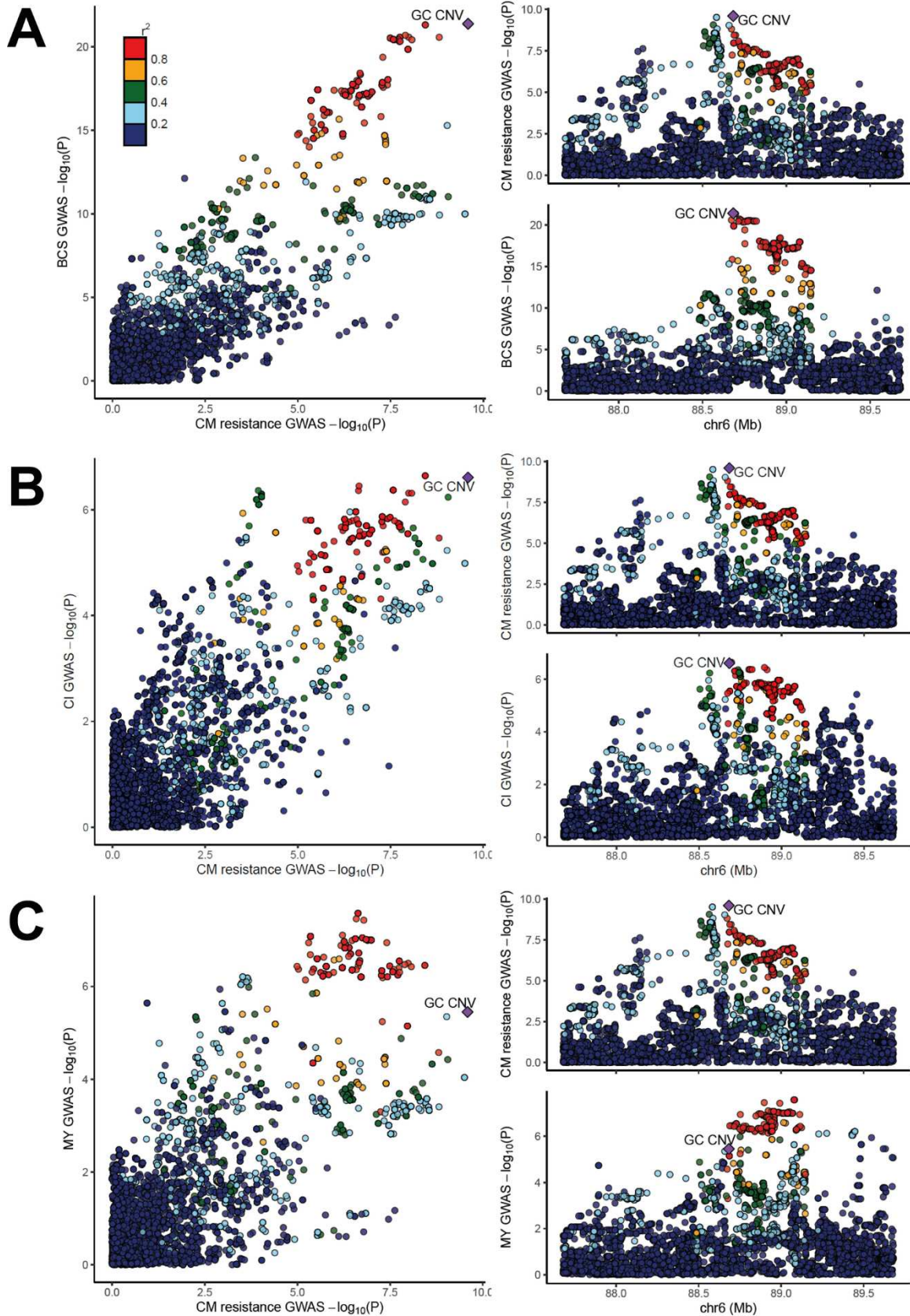


926
927
928



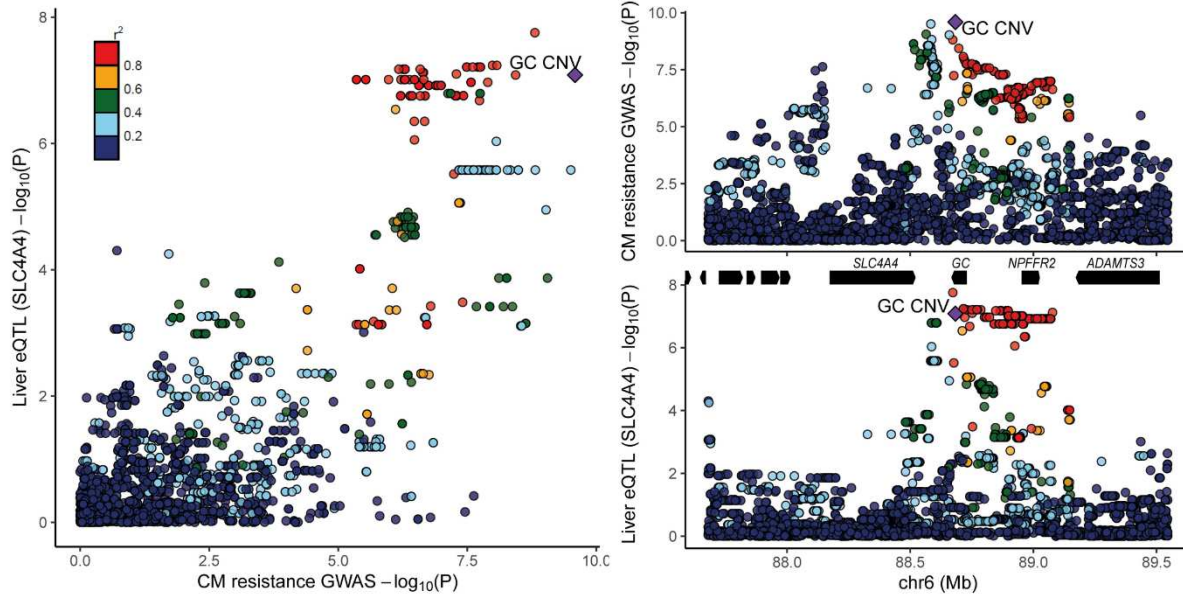
929
930
931

S5 Fig



932
933
934

S6 Fig



935
936
937
938 **S1 Table** Homozygosity-by-descent results
939 **S2 Table** GC CNV allele effects for CM resistance, milk yield, body condition score, and calving interval
940 **S3 Table** GC expression across various tissue types in human transcriptome databases
941 **S4 Table** Custom genotyping array probe design and genotyping results
942 **S5 Table** Summary-based Mendelian Randomization analysis results
943 **S6 Table** List of traits routinely collected in a Dutch HF breeding organization
944

945 **Data reporting**

946 Genome sequence data of the CM resistance QTL region (BTA 6:84-93 Mb) of the 266 Dutch Holstein Friesian animals are deposited
947 in the European Nucleotide Archive under accession [XXXX \(under preparation\)](#). The RNA-seq data is deposited under EBI
948 ArrayExpress accession E-MTAB-9348 and 9871. The genotype data used for eQTL mapping is deposited under [European Variant](#)
949 [Archive XXXX \(under preparation\)](#). The ATAC-seq data is deposited under EBI ArrayExpress accession E-MTAB-9872. Genotype and
950 phenotype data used for genome-wise association studies were obtained from CRV B.V., a commercial cattle breeding company. As
951 such, the data are available upon reasonable request and with permission of CRV B.V..

952

953 **Additional information requested at submission**

954 **Research Funding**

955 YLL, ACB, MB, MAMG, and RFV are financially supported by the Dutch Ministry of Economic Affairs (TKI Agri & Food project 16022)
956 and the Breed4Food partners Cobb Europe, CRV, Hendrix Genetics and Topigs Norsvin. CC and TD are senior research associates
957 from the Fonds de la Recherche Scientifique–FNRS (F.R.S.-FNRS). GCMM is post-doctoral fellow of the H2020 EU project BovReg
958 (2019-2022). This work was supported by grants from the European Research Council (Damona; ERC AdG-GA323030 to MG), and the
959 EU Framework 7 program (GplusE to MG and HT). YLL was supported by WIAS travel grant by Wageningen University and Research
960 and Erasmus+ grant for research visit.

961 The funders had no role in study design or decision to publish.

962

963 **Competing interests**

964 EM is an employee of CRV B.V., one of the partners of the Breed4Food consortium. All other authors declare that they have no
965 conflict of interest.

966